DOKUZ EYLÜL UNIVERSITY
GRADUATE SCHOOL OF NATURAL AND APPLIED SCIENCES

FATIGUE FAILURE ANALYSIS OF A HEAVY VEHICLE TRUCK WHEELS UNDER DYNAMIC LOADS BY RAINFLOW CYCLE COUNTING METHOD

by
Uğur POYRAZ

October, 2020
İZMİR

FATIGUE FAILURE ANALYSIS OF A HEAVY VEHICLE TRUCK WHEELS UNDER DYNAMIC LOADS BY RAINFLOW CYCLE COUNTING METHOD

A Thesis Submitted to the
Graduate School of Natural and Applied Sciences of Dokuz Eylül University
In Partial Fulfillment of the Requirements for the Degree of Master of Science
in Mechatronics Engineering

by
Uğur POYRAZ

October, 2020
İZMİR

M.Sc THESIS EXAMINATION RESULT FORM

We have read the thesis entitled **"FATIGUE FAILURE ANALYSIS OF A HEAVY VEHICLE TRUCK WHEELS UNDER DYNAMIC LOADS BY RAINFLOW CYCLE COUNTING METHOD"** completed by **UĞUR POYRAZ** under supervision of **ASSOC. PROF. DR. ŞAHİN YAVUZ** and we certify that in our opinion it is fully adequate, in scope and in quality, as a thesis for the degree of Master of Science.

……………………………………

Assoc. Prof. Dr. Şahin YAVUZ

Supervisor

……………………………………..

Prof. Dr. Hira KARAGÜLLE

(Jury Member)

..…………………………………

Assoc. Prof. Dr. Barış BIDIKLI

(Jury Member)

Prof. Dr. Özgür ÖZÇELİK

Director

Graduate School of Natural And Applied Sciences

ACKNOWLEDGEMENTS

First of all, I would like express my sincere gratitude to my supervisor Assoc. Prof. Dr. Şahin YAVUZ for the continuous support of my Master of Science study and research.

My sincere thanks also goes to Mr. Öztan ÖZTÜRK, R&D Manager at Maxion Wheels Jantaş Inc., and Mr. Serdar ERCAN Engineering Manager at Maxion Wheels Jantaş Inc. Manisa for giving this research subject, their extensive personal and professional guidance.

Besides, I also acknowledge Maxion Wheels Jantaş Company for giving me the opportunity to do this study and also the rest of my managers, collegues and friends. I am grateful and have a pleasure of being a member of this family.

Especially, I would like to thank my wife for her unconditional love, physical and mental infinite support.

Finally, I wish to thank to my parents and sisters for their love, endless support, encouragement throughout my life wholeheartedly.

Uğur POYRAZ

FATIGUE FAILURE ANALYSIS OF A HEAVY VEHICLE TRUCK WHEELS UNDER DYNAMIC LOADS BY RAINFLOW CYCLE COUNTING METHOD

ABSTRACT

Rainflow cycle counting method has a wide range of usage and is widely used for classification of data measured on products where fatigue tests and road performance data of vehicle components are collected.

In this study, strain data of heavy commercial vehicles under biaxial loads were evaluated using the rainflow counting method. In order to make this evaluation, strain gauges were applied to the heavy commercial vehicle wheel and the strain values were measured during fatigue test with different loading conditions. Three different wheel biaxial fatigue test machine also verified according measured strain data.

Keywords: Rainflow cycle counting method**,** fatigue, dynamic strain measurement

ÇEVRİM SAYMA METODU İLE AĞIR TİCARİ ARAÇ JANTLARININ DİNAMİK YÜKLER ALTINDAKİ YORULMA HASAR ANALİZİ

ÖZ

Yağmur akışı çevrim sayma metodu geniş kullanım alanına sahip olup yorulma testlerinin ve taşıtlardaki komponentlerin yol performans verilerinin toplandığı ürünler üzerinde ölçülen dataların sınıflandırılması için yaygınca kullanılmaktadır.

Bu çalışmada yağmur akışı çevrim sayma metodu kullanılarak ağır ticari taşıtların iki eksenli yükler altındaki gerinim verileri değerlendirilmiştir. Bu değerlendirmenin yapılabilmesi için ağır ticari taşıt jantına gerinim ölçerler yapıştırılarak farklı yükleme koşullarına sahip test esnasında gerinim değerleri ölçülmüştür. Değerlendirilecek olan gerinim veriler aynı zamanda üç farklı test makinasının doğrulama çalışmalarında kullanılmıştır.

Anahtar Kelimeler: Yağmur akışı çevrim sayma metodu, yorulma, dinamik gerinim ölçümü

CONTENTS

LIST OF FIGURES

Page

LIST OF TABLES

Page

CHAPTER ONE
INTRODUCTION

The steel wheel is located as a circle shape inside the tire on a commercial vehicle. Generally, heavy commercial vehicle wheels made by steel. The vehicle can be moved by mounting a tire around the wheel. The wheels, which are an important element in the exterior of the vehicle, are directly connected to the axle system. By this way wheels transmit vertical and lateral road forces to vehicle chassis through the axle. Wheels are considered critical parts in the automotive industry due to their area of usage. Problems may arise due to the wrong wheel design such as load capacity issues, fuel consumption inefficiency and vehicle dynamic problems. Therefore, the verification of the tests to be performed is of great importance.

Studies on steel wheel fatigue life and test method have gained speed especially in the last forty years. In 1983, Grubisic & Fischer from Fraunhofer - Institut für Betriebsfestigkeit published their work on wheel fatigue life, design and test method under radial and lateral operating loads (Grubisic & Fischer, 1983).

In 2003, Carboni, Beretta & Finzi conducted a study on the fatigue behavior of steel rim material and investigated air hole design damage (Carboni, Beretta, & Finzi, 2003).

Topaç, Ercan & Kuralay studied on fatigue life prediction of a heavy vehicle steel wheel under radial loads by using finite element analysis (Topaç, Ercan, & Kuralay, 2012).

In this study, a method that will guarantee the accuracy of the rim design verification test machines will be studied. These studies also shed light on the future wheel finite element calculations to be used in the correlation studies of the test data and finite element simulations.

CHAPTER TWO
COMMERCIAL WHEEL PRODUCTION STAGES

2.1 Wheel Manufacturing

The manufacturing process of steel wheels manufactured for use in commercial vehicles generally consists of 4 stages. These stages are; manufacture of separate rim and disc parts, followed by the assembly process connecting these two basic parts, and finally the paint process, which protects the wheel construction from external influences and possible corrosion.

In this section, the effects on the fatigue life will be examined by focusing on the steel wheel manufacturing stages. However, since the constructive manufacturing stages that affect fatigue life will be detailed, the paint process will not be emphasized.

2.2 Rim Production Processes

The hot rolled sheet steel in roll form, which is supplied by steel sheet manufacturers and enters the manufacturing area, enters the roll opening and slicing machine as the first process. In this process, the sheet metal, which is sliced transversely, is subjected to blasting process in order to eliminate the scales that may occur on the surface during shipment and storage. After this stage, rim marking and length cutting in accordance with the size of the rim to be produced are performed and the rim material preparation part of the manufacturing process is completed.

The rectangular sheet metal sheet with the appropriate width, length and thickness is sent to the predetermined rim line and undergoes rounding and face straightening operations, respectively. In these processes, the sheet metal rolled on the roll is prepared for the butt-welding operation. In the steel rim manufacturing sector, resistance butt welding or flash-welding butt welding is generally preferred as butt welding process.

The sheet metal, whose corners are joined with the butt-welding operation, after enters the scarfing, edge cutting and scrubbing machines, respectively, in order to remove the excess metal overflowing from the butt area during the welding process. After these operations, the re-rounding operation is carried out to give the sheet plate a circle shape again and then it is sent to the pre-bending process, which is applied to pre rim form profiles on the rim.

The rim which comes out of the pre-bending process is passed through 3 rim rolling operations in a row and the profiles on it are provided to appear in the desired dimensions which is shown in Figure 2.1. After this stage, the rim enters the calibration press in order to give the appropriate diameter size and then takes its final shape with the valve hole drilling and punching operation.

Figure 2.1 Rim flow forming process (Personal archive, 2020)

After valve hole drilled and punched rim is sent to the assembly line after it is visually and dimensionally checked. Process flow chart of rim manufacturing is given in Figure 2.2 and the appearance of a completed rim is given in Figure 2.3.

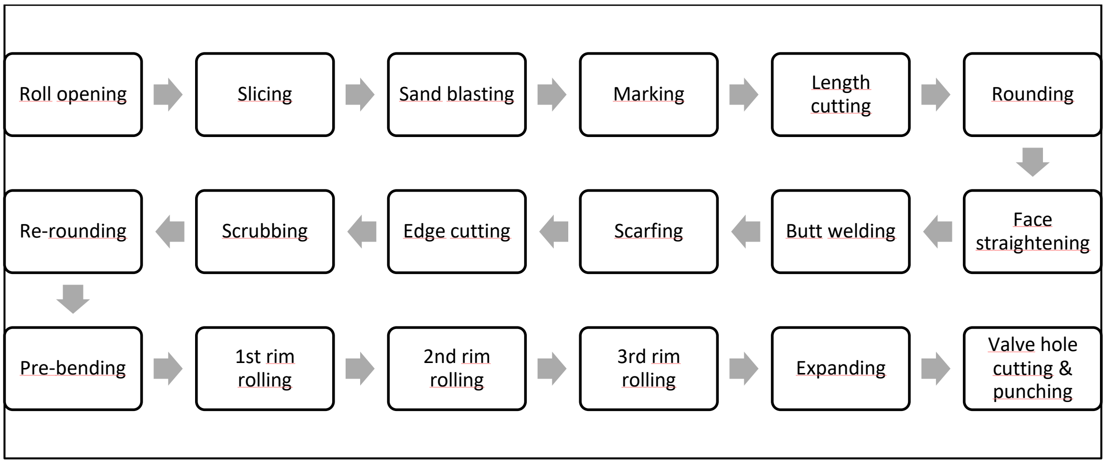

Figure 2.2 Rim process flow diagram (Personal archive, 2020)

Figure 2.3 Finished rim part (Personal archive, 2020)

2.3 Disc Production Process

As same as rim manufacturing process, the disc material is cut square after the material checked quality control, unrolling, length cutting and sandblasting. After that, the square cut material is cut circularly in the press to the desired dimensions starting of disc production line. The process called ear cutting and sent to the appropriate disc production line.

Disc material is first subjected to flow forming process in the production line given in Figure 2.4. As a result of this process, the disc material gets its basic profile. Another feature of this process is that thanks to flow forming, it provides significant strengthening in certain areas of the material and increases the strength in flow formed regions.

Figure 2.4 Disc flow forming process (Personal archive, 2020)

After this process, punching of the stud holes and the hub diameter that provides the connection of the wheel to the vehicle axle is performed. Subsequently, the drilling of ventilation holes, which serve to cool the brake drum, is applied. At this stage, ventilation hole coining operation, which is the second operation related to ventilation holes, is performed. As seen in radial fatigue tests, the area in which a disc is generally subject to fatigue damage is around the vents. Therefore, it is of great importance for the fatigue life of the disc construction to reduce the stress concentration caused by the notch effect in this region and to increase the fatigue life.

After the above steps, bolt hole coining is performed to eliminate the notch effect and disc straightening operations are carried out to ensure parallelism on the disc surface. After these processes, turning operations, which will bring the disc to its final dimensions, are started. These operations applied on CNC machines; are the turning operations that will finalize the disk length, disc leg outer diameter and center diameter. Then the disc is sent to the relevant assembly line by applying the washing process. The process flow chart of disc manufacturing is given in Figure 2.5 and the appearance of the disc with completed manufacturing is given in Figure 2.6.

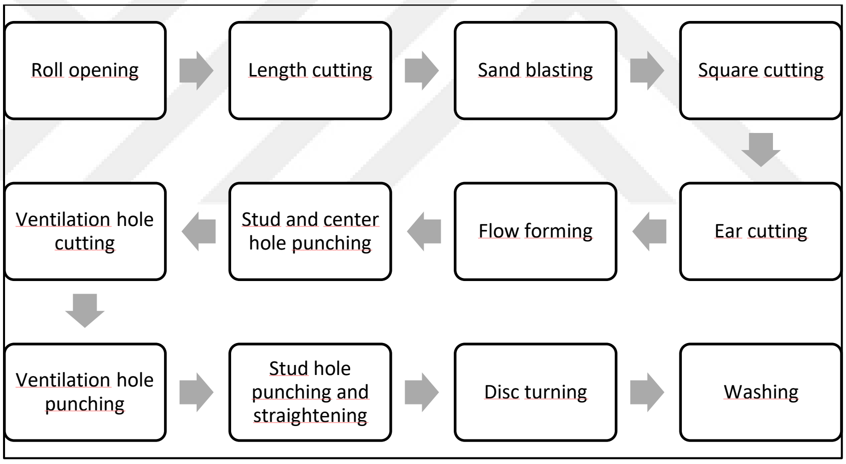

Figure 2.5 Disc process flow diagram (Personal archive, 2020)

Figure 2.6 Finished disc part (Personal archive, 2020)

2.4 Assembly Process

Rim and disc coming from the production lines are combined in the relevant assembly line as a tight fit with the assembly press. Subsequently, it is transferred to the secretory measuring station on the conveyor, measured and tapped so that this setting is not disturbed. After the submerged arc welding source connecting the rim and the disc which is given in Figure 2.7, the mounted wheel is sent to the CNC lathe by applying cooling and straightening operations, respectively. Here, internal and external surface lathes of the disc part of the rim are made, after which a marking operation is performed, which precisely indicates the properties of the rim. After performing the run-out and visual-dimensional controls of the wheel, the wheel is sent to the paint process. Assembly process flow is shared Figure 2.8.

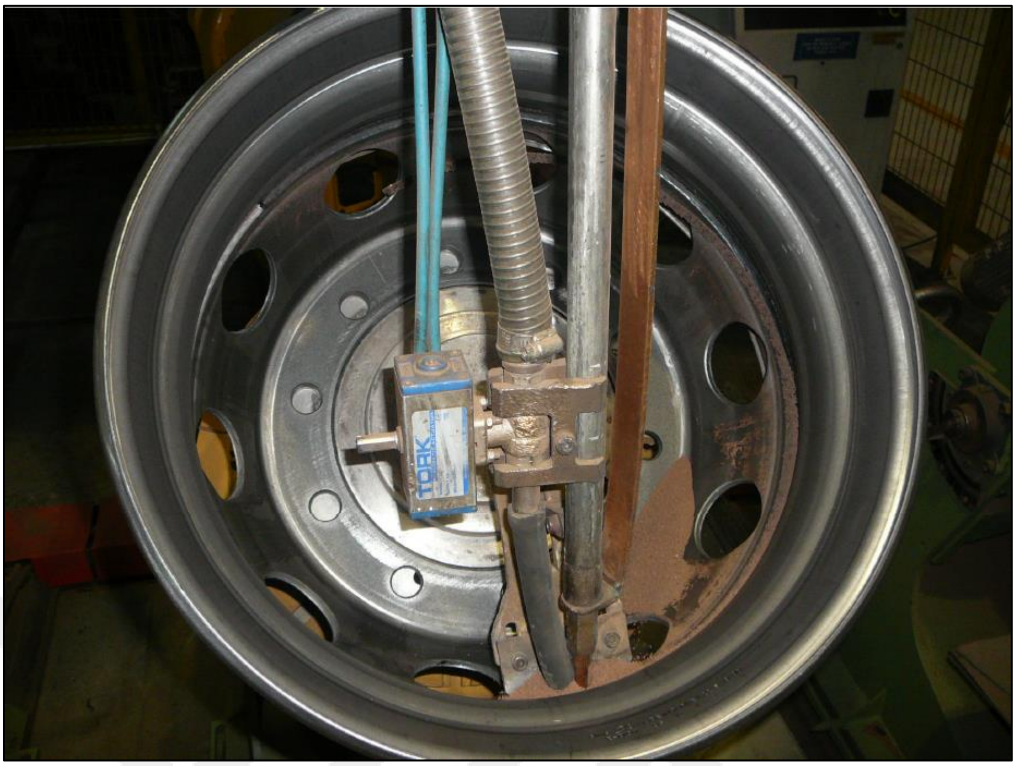

Figure 2.7 Wheel assembly welding process (Personal archive, 2020)

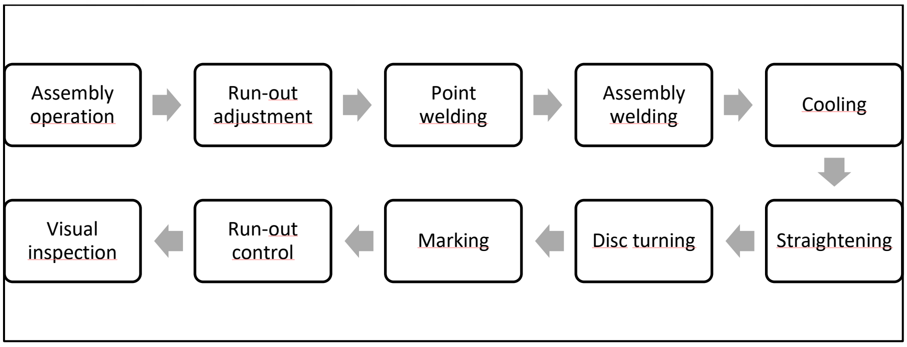

Figure 2.8 Wheel process flow diagram (Personal archive, 2020)

CHAPTER THREE
WHEEL CONSTRUCTION AND MATERIAL

3.1 Construction Properties

In general, the rim consists of three main elements. The connection between the vehicle and the road is ensured by mounting the tire on the rim. The connection of the wheel with the vehicle is made by mounting the disc and the vehicle hub. Also disc part has ventilation holes that benefits for cooling vehicle break system. The valve is the element where the required air pressure is applied to the tire-wheel assembly.

The general view of a commercial vehicle wheel showing the basic parts is shown in Figure 3.1.

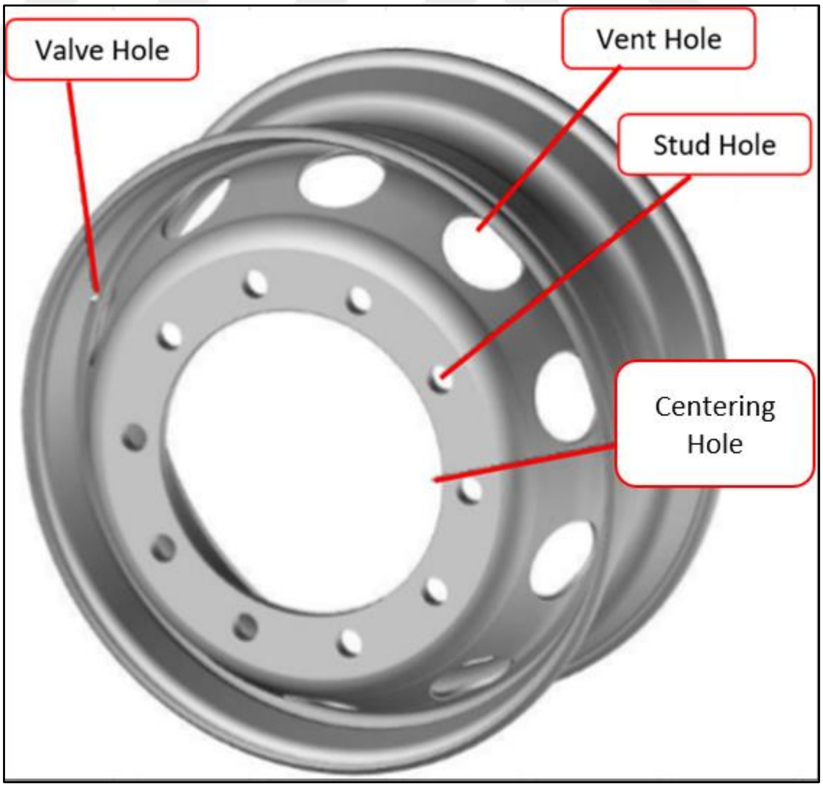

Figure 3.1 Wheel construction (Personal archive, 2020)

3.2 Material Properties

The casting type of the steel used in the production of wheels is continuous while the rolling type is hot rolling. The internal structure features of the steel sheet coming to the production area in rolls and an exemplary internal structure photograph of RSt 52-3 steel with 200 magnification is given Figure 3.2.

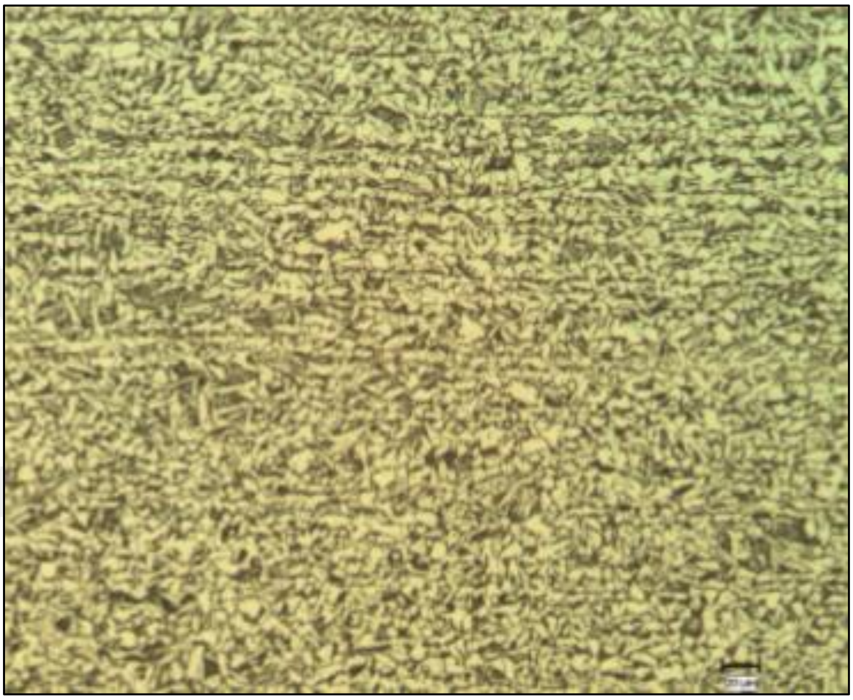

Figure 3.2 RSt-52 material microstructure (Ercan, 2011)

The general properties that rim manufacturing steel should have are as follows.

- Hot rolled rim steel should be of uniform, ferritic pearlitic structure with no intergranular cementite.
- According to EN 103-71, ferrite grain size must be 7 or smaller.
- Steel should be suitable for submerged and submerged arc welding methods for the assembly process.
- For the disc manufacturing process, it must be suitable for resistance welding and burning butt welding methods.

- It should be suitable for cold forming and cold plastering method with its high elongation characteristic.

The chemical and material properties of the wheel materials are given in the Table 3.1, Table 3.2, Table 3.3, Table 3.4.

Table 3.1 Rim material chemical composition (Ercan, 2011)

Material	C max	Si max	Mn max	P max	S max	N max
	0.1	0.15	1.6	0.02	0.08	90ppm
S460MC	Al	Cu+Cr+Ni max	Sn max	Nb max	Ti max	
	0.02-0.06	0.2	0.01	0.09	0.22	

Table 3.2 Rim material mechanical properties (Ercan, 2011)

Material	R_e (MPa)	R_m (MPa)	e_{min} (%)
S460MC	450-550	550-650	24

Table 3.3 Disc material chemical composition (Ercan, 2011)

Material	C max	Si max	Mn max	P max
	0.19	0.3	1.6	0.02
RST 52-3 S355J2G3C	S max	N max	Al	Cu+Cr+Ni max
	0.015	90ppm	0.025-0.065	0.3

Table 3.4 Disc material mechanical properties (Ercan, 2011)

Material	R_e (MPa)	R_m (MPa)	e_{min} (%)
RST 52-3 S355J2G3C	330-410	480-570	25

CHAPTER FOUR
WHEEL FATIGUE TEST TYPES & STANDARDS

4.1 Introduction

Fatigue life of wheels used in commercial vehicles are generally determined in three ways with the help of radial fatigue test, corner fatigue test and biaxial fatigue test.

The mentioned fatigue tests of the manufactured prototype wheels are the international Association of European Wheel Manufacturers [EUWA] - ES 3.11, ES 3.23, Society of Automotive Engineers [SAE] - J267, Japanese Industrial Standard [JIS] - D 4103 or according to the vehicle manufacturers own standards. Today, vehicle manufacturers generally use EUWA in Europe, SAE in the U.S. and JIS in Japan. In addition to these international standards, fatigue-tested wheels must provide a number of additional features and conditions set by vehicle manufacturers (Ercan, 2011).

4.2 Radial Fatigue Test

In the radial fatigue test; The prototype rim is tested with the tire mounted on it and inflated with a certain air pressure and is rotated at a certain speed by applying the radial force calculated in the standards. During this process, the front wheel or camber angle is not given to the rim. A schematic drawing of the radial fatigue test rig is given in Figure 4.1, and a sample wheel on the test rig and the overall appearance of the tire is given in Figure 4.2.

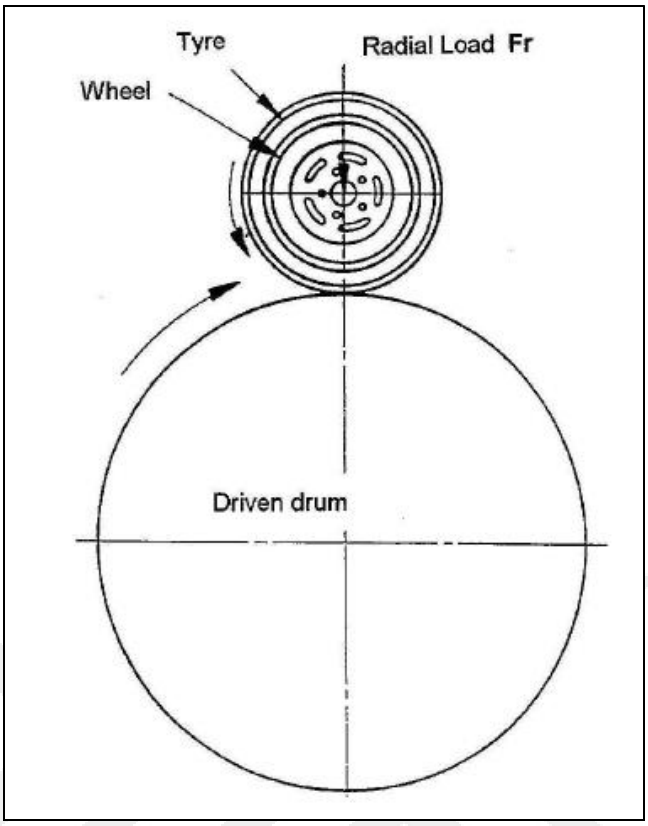

Figure 4.1 Radial fatigue test machine schematic drawing (Association of European Wheel Manufaturers, 2006)

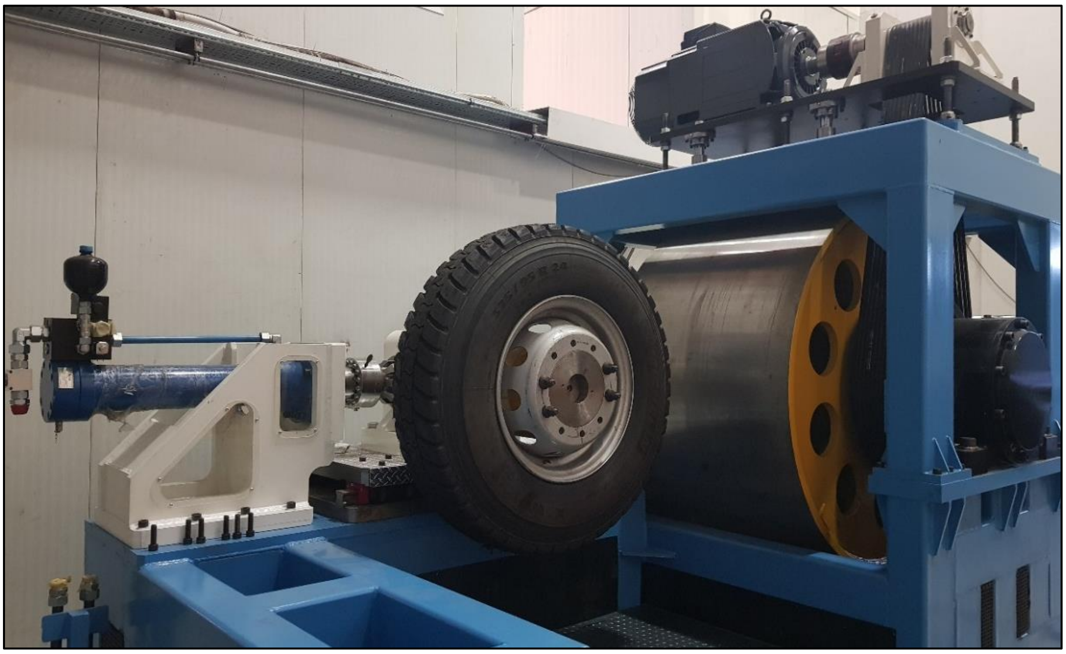

Figure 4.2 Radial fatigue test machine (Personal archive, 2020)

The Fr force applied on the wheel during the test is calculated as the product of the wheel load capacity by the coefficient given in the relevant standard in equation (Equation 4.1).

$$\mathrm{Fr} = \mathrm{F} * \mathrm{k} \tag{4.1}$$

Fr [N] = Test load

Fv [N] = Wheel load capacity

k [-] = Accelerated test load factor

After the force is adjusted, the wheel, the tire consisting of the tire inflated with the air pressure given in the standards and the representative axle, slides automatically on the machine axis, is pressed into the free-rotating drum and the rotation is started. The test is stopped at predetermined intervals by the company and damage inspection is performed especially on critical sections on the wheel. The radial fatigue test is then continued until a start of fatigue damage is detected on the wheel. The number of revolutions at which the onset of damage occurs results in the fatigue life of the wheel under test under specified conditions. If this fatigue life is more than the minimum cycle given in the relevant standard, the wheel succeeds radial fatigue test.

4.3 Cornering Fatigue Test

The corner fatigue test is applied to determine the dynamic strength and fatigue life of the wheel against the lateral loads and moments that the wheel will be exposed to while driving. In this test, the rim is fixed without tire with the help of special apparatus to the test machine flange and applied to a bending moment system given in the standards with the help of a shaft perpendicular to the plane of the hub. In this way, the wheel is applied repeated bending moment. The wheel is checked periodically checked if fatigue crack is occurred or not. In the number of revolutions at which the onset of fatigue damage is observed, the test is terminated and the fatigue life is determined. The schematic drawing of the test machine is given in Figure 4.3 and the general view is given in Figure 4.4.

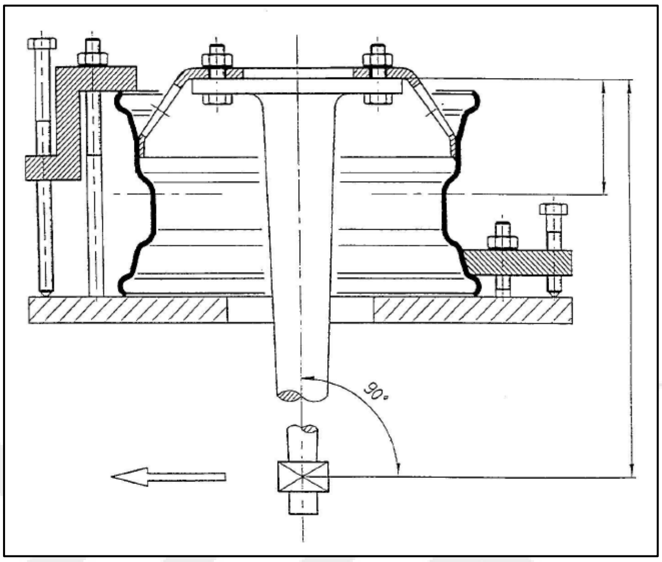

Figure 4.3 Cornering fatigue test machine schematic drawing (Association of European Wheel Manufaturers, 2006)

Figure 4.4 Cornering fatigue test machine (Personal archive, 2020)

The bending moment to be applied to the wheel in the corner fatigue test is calculated by the formula below.

$$M = (\mu . Rdyn + d) . Fv . S \tag{4.2}$$

Where;

- μ [-] : is the assumed coefficient of friction developed between tire and road; for tires on drop centre rims use "μ = 0.7", for tires on bead seat rims use "μ = 0.65"
- Rdyn [m] : is the dynamic loaded radius defined as the circumference divided by 2π of the largest tire to be used on the wheel as specified by the vehicle or wheel manufacturer.
- d [m] : Wheel inset/ofset
- Fv [N] : Wheel load capacity
- S [-] : Accelerated test factor

4.4 Biaxial Fatigue Test

Wheels, hubs and bolts are highly relevant for the operational safety of passenger cars and commercial vehicles so these parts must not fail even at harsh usage and minimum maintenance. The most cost and time efficient approach for the durability performance approval is an accelerated life test using service load simulation. Therefore, a laboratory-based environment for the whole assembly and realistic load interaction provides unrivalled results for durability and operational safety.

Vehicle manufacturers pay attention to durability tests. However, these tests need to be carried out under real road conditions and are time-consuming studies. Also, these activities are expensive. For this reason, it needs to be able to represent the real road conditions in a short time and cost less test methods.

Work on establishing a mechanism to represent real road conditions in the laboratory environment began in the early 1960s. The biaxial wheel fatigue test has been used successfully since the early 1980s. It is an internationally accepted test method for design verification of newly designed commercial vehicle wheels. This test method was developed by Fraunhofer LBF which is the world's leading fatigue and endurance institute. Today, this technology is used by leading vehicle manufacturers such as Daimler, Volvo, and MAN (BiAx Wheel Test Technology, n.d.).

The wheel assembly is loaded by vertical and lateral actuators which are capable to represent real road conditions. To guarantee the similar conditions experienced by a vehicle in service. Schematic description of biaxial fatigue test machine is given Figure 3.5 and Maxion Wheels Jantaş Inc. Biaxial fatigue test machine schematic drawing is given Figure 4.5 and Jantaş biaxial fatigue test machine picture is given Figure 4.6.

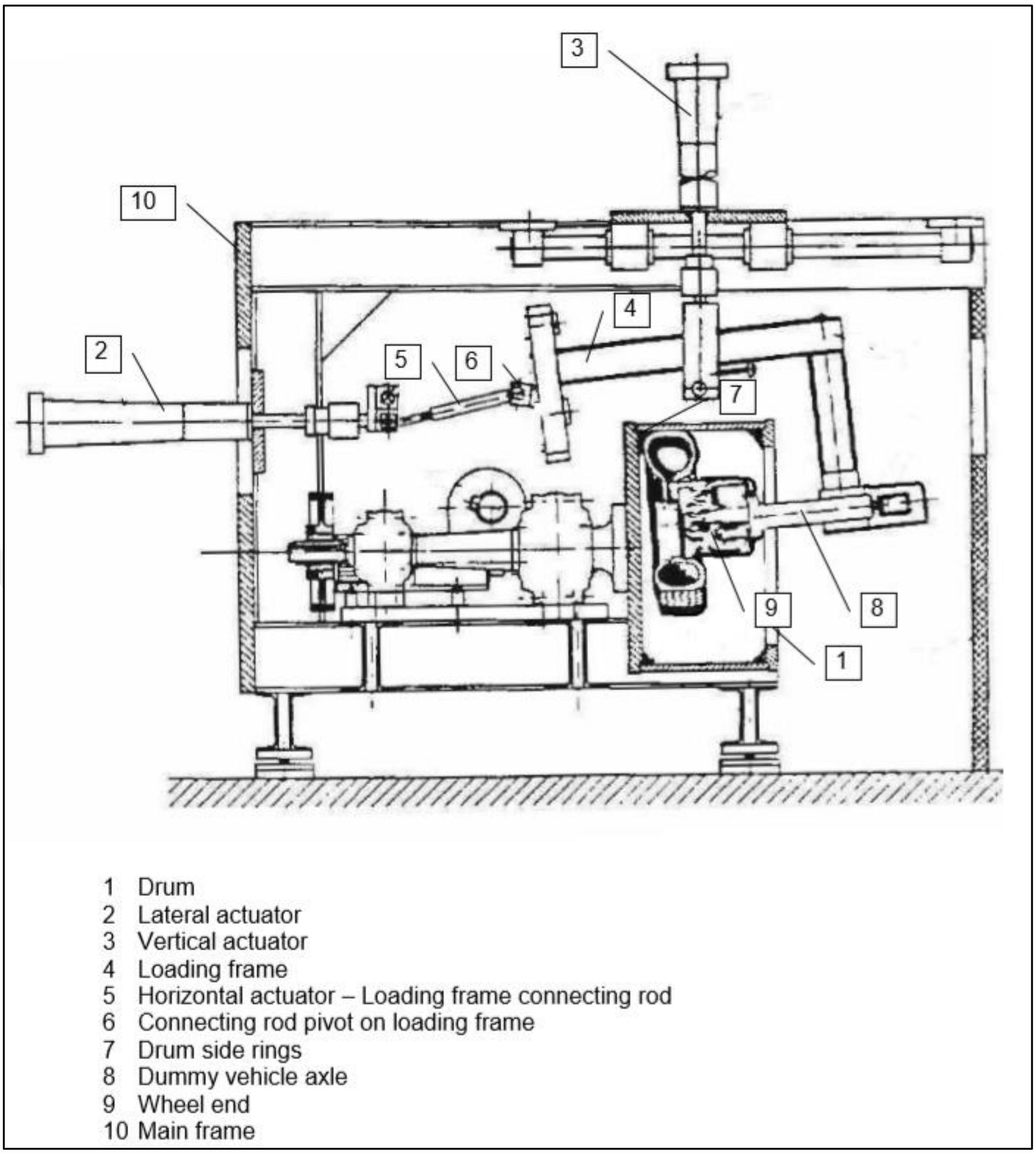

Figure 4.5 Biaxial fatigue test machine schematic drawing (Association of European Wheel Manufaturers, 2017)

The wheel is attached to the test vehicle hub as shown in the schematic picture. The loading program is created on the computer according to the carrying load capacity of the wheel. Turning drum is representing the road, the test is carried out by being exposed to vertical and horizontal forces in accordance with the loading program. The forces defined in this loading program are obtained through vertical and horizontal hydraulic actuators. And the test is repeated until test termination criteria provided.

Figure 4.6 Biaxial fatigue test machine (Personal archive, 2020)

Most major commercial vehicle manufacturers require the test standard "E S 3.23 BIAXIAL FATIGUE TEST FOR TRUCK WHEELS" published by the Association of European Wheel Manufacturers [EUWA] for wheel design approval.

In Table 4.1, the basic loading program called "Eurocycle", which shows 98 loads of loading conditions, is shown in the biaxial test according to E.U.W.A. ES 3.23 standard.

Table 4.1 Biaxial fatigue test base load programme (Association of European Wheel Manufaturers, 2017)

SQ	Cycle	Fv [kN]	Fh [kN]
1	100	37.5	0.00
2	40	50.0	27.50
3	85	25.0	7.50
4	230	37.5	0.00
5	40	62.5	29.00
6	40	37.5	0.00
7	30	58.0	32.00
8	95	32.5	-7.50
9	80	52.5	24.00
10	95	25.0	-7.50
11	85	50.0	27.50
12	300	37.5	0.00
13	195	38.8	15.00
14	75	31.0	0.00
15	75	46.0	21.00
16	55	25.0	-10.00
17	205	37.5	10.00
18	60	70.0	20.00
19	80	50.0	23.00
20	55	22.5	-7.50
21	170	37.5	2.50
22	70	55.0	25.00
23	20	55.0	25.00
24	110	35.0	-3.75
25	30	35.0	10.00
26	25	50.0	30.00
27	150	35.0	-6.25
28	20	70.0	32.00
29	150	35.0	0.00
30	50	65.0	30.00
31	130	42.5	0.00
32	65	65.0	12.00
33	65	65.0	-12.00
34	65	45.0	6.00
35	65	45.0	-6.00
36	65	65.0	0.00
37	65	42.5	0.00
38	4325	35.0	0.00
39	35	55.0	25.00
40	115	35.0	-10.00
41	130	40.0	7.50
42	20	40.0	18.00
43	65	32.5	0.00
44	30	40.0	22.50
45	250	32.5	0.00
46	45	50.0	27.00
47	75	37.5	5.00
48	35	30.0	-10.00
49	60	37.5	5.00
50	35	25.0	-10.00
51	70	37.5	0.00
52	30	85.0	39.00
53	105	34.0	-7.50
54	30	55.0	25.00
55	40	42.5	10.00
56	25	50.0	28.00
57	15	25.0	-10.00
58	35	35.0	0.00
59	25	25.0	-10.00
60	15	40.0	18.00
61	55	30.0	-10.00
62	30	55.0	27.50
63	15	30.0	-10.00
64	80	40.0	0.00
65	55	30.0	-10.00
66	45	55.0	27.50
67	25	25.0	-10.00
68	60	40.0	0.00
69	30	25.0	-10.00
70	50	40.0	0.00
71	20	55.0	27.50
72	45	30.0	0.00
73	50	60.0	27.50
74	130	42.5	0.00
75	65	65.0	12.00
76	65	65.0	-12.00
77	65	45.0	6.00
78	65	45.0	-6.00
79	65	65.0	0.00
80	65	42.5	0.00
81	65	40.0	0.00
82	45	25.0	-10.00
83	70	50.0	23.00
84	240	35.0	10.00
85	40	55.0	25.00
86	4300	54.0	0.00
87	15	70.0	32.00
88	75	40.0	10.00
89	105	25.0	-10.00
90	600	35.0	0.00
91	40	40.0	15.00
92	50	40.0	0.00
93	30	50.0	15.00
94	40	35.0	-10.00
95	20	40.0	20.00
96	15	25.0	-10.00
97	15	45.0	21.00
98	170	37.5	0.00

Most important testing parameters are vertical and lateral force coefficients (Cv and Cl). To adapt the basic program to the specific vehicle multiply basic program loads by the corresponding coefficient (Cv or Cl). Table 4.2 shows Cv and Cl values according to E.U.W.A. 3.23 standard.

Table 4.2 Biaxial fatigue Cv and Cl coefficient table (Association of European Wheel Manufaturers, 2017)

Load Program	Wheel	Fstat[kN]	Cv	Cl	Tyre
LBF 1	17.5"x6.00	16.5	0.55	0.47	225/75 R 17.5
LBF 1	17.5"x6.75	17	0.57	0.49	225/75 R 17.5
LBF 1	17.5"x6.75	18.5	0.61	0.52	225/75 R 17.5
LBF 1	17.5"x6.75	21.2	0.7	0.6	235/75 R 17.5
LBF 1	17.5"x6.75	23.6	0.75	0.65	235/75 R 17.5
LBF 1	19.5"x6.75	25	0.75	0.65	265/70 R 19.5
LBF 1	19.5"x7.50	28	0.8	0.75	285/70 R 19.5
LBF 1	19.5"x7.50	29	0.83	0.78	285/70 R 19.5
LBF 1	19.5"x8.25	30	0.85	0.8	305/70 R 19.5
LBF 1	19.5"x8.25	31.5	0.89	0.84	305/70 R 19.5
LBF 1	19.5"x8.25	30.75	0.87	0.82	305/70 R 19.5
LBF 1	22.5"x7.5	35.5	1.2	1.2	275/70 R 22.5
LBF 1	22.5"x7.5	32.5	1.1	1.1	275/70 R 22.5
LBF 1	22.5"x8.25	35.5	1.2	1.2	295/80 R 22.5
LBF 1	22.5"x9.00	40	1.3	1.25	315/80 R 22.5
LBF 1	22.5"x9.00	41	1.33	1.28	315/80 R 22.5
LBF 1	22.5"x11.75	45	1.46	1.41	385/65 R 22.5

The load program shall be repeated until test termination. Biaxial fatigue test acceptance requirements according to E.U.W.A. 3.23 are given in Table 4.3.

Table 4.3 Biaxial fatigue test acceptance requirements (Association of European Wheel Manufaturers, 2017)

Material	Diameter	Design Life	Nr. Of Tests	Test Life	Test Termination
Ferrous	D = 17.5"	600,000 km	2	12,000km	Wheel in full functionality. Short technical cracks allowed.
			1	18,000km	Wheel in full functionality. Short technical cracks allowed.
	D > 17.5"	1,000,000 km	2	16,000km	Wheel in full functionality. Short technical cracks allowed.
			1	24,000km	Wheel in full functionality. Short technical cracks allowed.
Aluminium alloy	D = 17.5"	600,000 km	2	15,000km	Wheel in full functionality. Short technical cracks allowed.
			1	22,500km	Wheel in full functionality. Short technical cracks allowed.
	D > 17.5"	1,000,000 km	2	20,000km	Wheel in full functionality. Short technical cracks allowed.
			1	30,000km	Wheel in full functionality. Short technical cracks allowed.

4.5 Wheel Fatigue Test Machines Control And Calibration Procedures

The wheel designs, which are shown as one of the safety parts in the automotive sector, are verified by the fatigue tests shared in the previous sections. It is of great importance that the accuracy of these tests is periodically checked and reported.

The E.S. 3.29 “CHECK AND CALIBRATION PROCEDURES FOR FATIGUE TEST BENCHES OF WHEEL” procedure published EUWA describes the control and calibration procedures of wheel fatigue test benches.

In this study, dynamic control and stress analysis comparison procedure, which is the 4th procedure from 4 different control procedures according to EUWA E S 3.29, will be discussed. Control procedures according to EUWA E S 3.29 are shared in Table 4.4.

Table 4.4 Wheel fatigue test machine control procedures table (Association of European Wheel Manufaturers, 2017)

Procedure ID	#1	#2	#3	#4
Check Type	Static	Static	Dynamic	Dynamic
Load Chain Checked	Partial	Complete	Complete	Complete
Complexity of Execution	LOW	LOW	HIGH	HIGH
Execution Costs	LOW	LOW	HIGH	LOW
Required Skill	LOW	LOW	HIGH	HIGH
Correct error cause by Dynamic Controller Device Stability	NO	YES	YES	YES
Correct error cause by dynamic effects (inertia, friction, clearances, …)	NO	NO	YES	YES
Correct error cause by mechanical set-up, misalignment	YES	YES High risk	YES	NO
Correct error cause by sensor mass and stiffness	NO	YES	YES High risk	NO
Test bench calibration	YES	YES	YES	NO

4.5.1 Dynamic Bench Check by Stress Analysis

This control procedure is generally used to check the biaxial fatigue testing machines. The procedure is generally based on the principle of comparing a slave machine with a known accuracy master machine.

In order to perform this process, strain gauge is applied on a wheel. The measurement wheel with the strain gauge applied is first connected to the test machine of which accuracy is known. In order to minimize the thermal effects, a test is should run for warm up at least 1 Eurocycle. Then a data acquisition device is placed on the wheel. The data acquisition device used herein can be telemetric capable of transmitting wireless data or embedded system which can save data to its storage memory. Then 1 Eurocycle of data is collected. This process is done in the same way that the machine is to be checked and all the data to be compared.

According to EUWA E.S. 3.29, when applying the dynamic control and stress analysis comparison procedure, a minimum 4 strain gauge should be applied to the measuring wheel and the sample rate frequency should be capable of collecting 36 data at 1 cycle of the wheel. Dynamic control and stress analysis comparison procedure schematic drawing is shown in Figure 4.7.

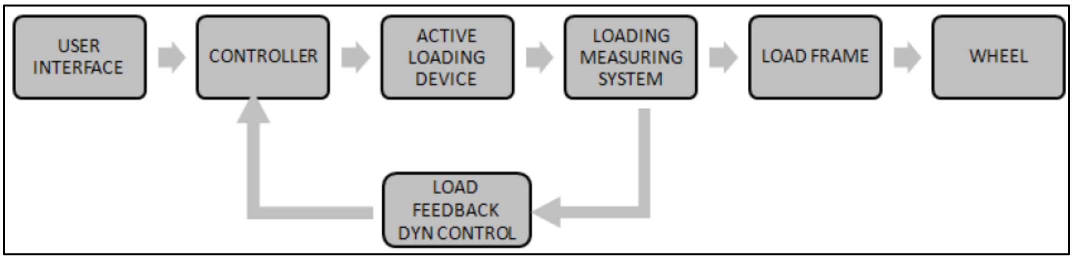

Figure 4.7 Dynamic control procedure schematic drawing (Association of European Wheel Manufaturers, 2017)

Since there will be a single loading condition in the radial fatigue test and corner fatigue tests, comparison can be made by looking at the stress amplitude in these tests. However, since there will be different load cases and the number of data collected for the biaxial fatigue testing machine will be quite high and complex, a description has been made in EUWA E S 3.29 for the evaluation of these data. This definition called as RFS which is acronym of Required fatigue stress.

Given a structure subjected to a variable loading, each point of the structure will be subjected to a stress time history. By stress cycle counting, the stress time history is reduced to sequence of pairs number of cycles – stress amplitude: n_i - Sa_i. This representation is called the stress amplitude spectrum. The fatigue material behavior is characterized by bilinear S-N curve as follow:

- Slope for over the fatigue limit = $K = -\frac{\Delta\log(N)}{\Delta\log(Sa)}$
- Slope for below the fatigue limit = $K_1 = -\frac{\Delta\log(N)}{\Delta\log(Sa)}$
- Fatigue limit = N_{fl}
- Fatigue limit stress = Fl

For each pair of stress amplitude spectrum, the damage d_i is calculated as:

- $d_i = n_i / N_i$. Where N_i is the number of cycles relevant to Sa_i on the S-N curve.

The damage sum D is the sum of all d_i. The target damage D_T represents the limit at which the material will fail. RFS is the local fatigue limit Fl of the material that leads to the target damage D_T. Here follows the description of RFS calculation procedure fixing all parameter needed to have comparable results. RFS value can be calculated only in an iterative way. RFS calculation steps given in Figure 4.8.

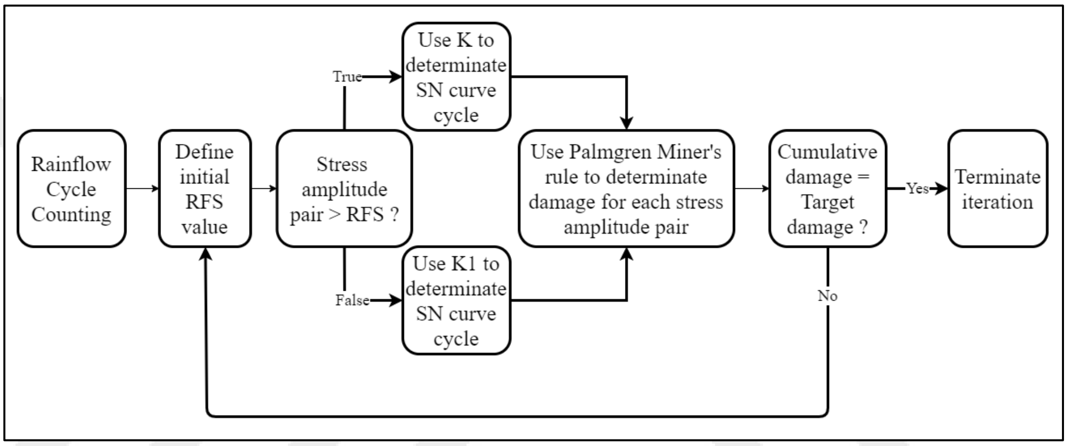

Figure 4.8 RFS calculation steps schematic drawing (Personal archive, 2020)

In case stress data are derived from strain measurements, Young modulus is obtained 210GPa for steel material. And Rainflow Cycle Counting method is applied according to ASTM E 1049-85.

S-N curve parameters are predicted as over the fatigue limit K=5.5, below the fatigue limit K1=10, and fatigue limit is selected Nfl= $2*10^6$ accrding to E.U.W.A. ES 3.29. Target damage is chosen as 0.5.

Stress amplitude spectrum classified with respect to precision of 0.1% of maximum stress cycle or better. Required fatigue stress calculation iteration converged should be less than %0.001 for RFS.

This dynamic bench check procedure will be applied in upcoming chapters after strain measurement studies.

CHAPTER FIVE
FATIGUE THEORY

5.1 History Of Fatigue

Sir Robert Hooke proposes the Hooke law in 1678, which establishes a linear relationship between stress and strain.

The fatigue word emerged in 1839 when Jean-Victor Poncelet was used for the first time in mechanics books. Poncelet produced mill axle equipment with cast iron. According to observations, these equipments were broken after a certain use. The fatigue word was put forward by himself as a result of these observations.

In 1842 Versailles train accident is usually shown as the beginning of understanding the cyclical fatigue mechanism. In this locomotive crash, which resulted in the death of more than 50 people, the axle was unexpectedly broken. Cyclical loads at low amplitudes in those years could not be predicted to lead such this kind of failure.

Figure 5.1 Versailles train crash (Versailles rail accident, n.d.)

In 1867 at the Paris Conference August Wöhler presents fatigue behavior of metal materials and their curves. The curves will later be called Wöhler Curves. With the help of these curves, the Versailles train crash accident had become better interpreted. Wöhler developed a basic test bench to apply repeated loads to railroad axles. The relationship between number of accumulated of failure cycle and load level is revealed by his study.

The effect of mean stress and stress amplitude relationship on fatigue life was established in 1899 with the Goodman-Haigh diagram (Figure 5.2). This diagram shows the relationship between the region representing the infinite life and the mean stress-stress amplitude.

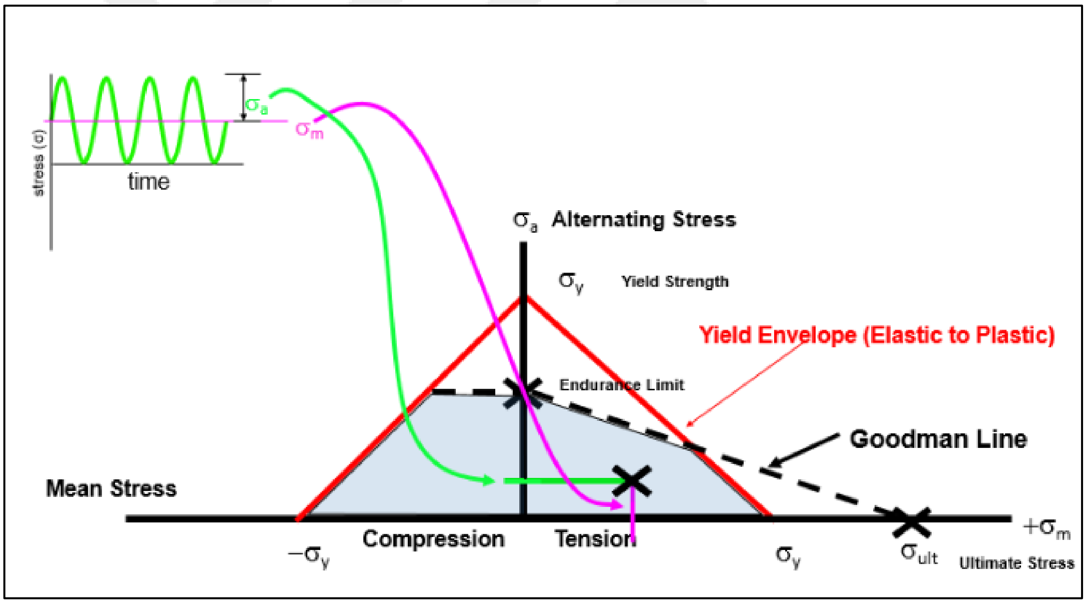

Figure 5.2 Goodman - Haigh diagram (History of Fatigue, n.d.)

In 1910 O.H. Basquin discovered a logarithmic relationship between stress amplitude and fatigue life on Wöhler Curves (Figure 5.3). This relationship means that a small change in stress level causes a big difference on life.

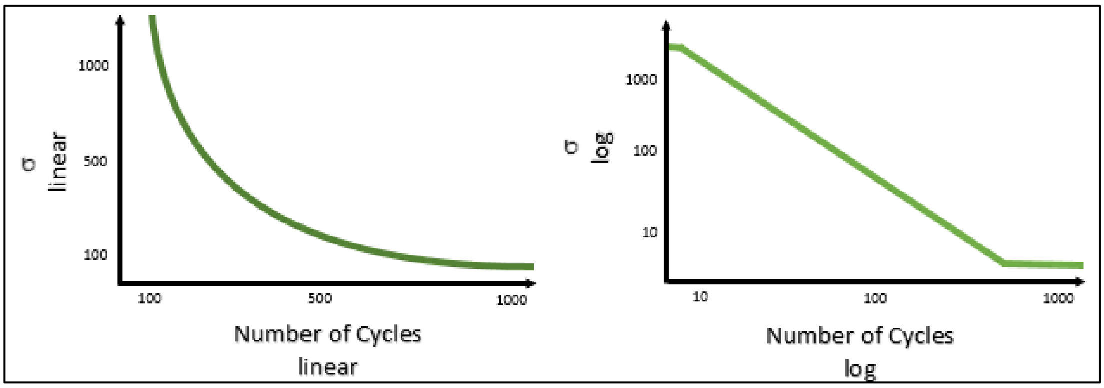

Figure 5.3 Linear versus log-log relationship of number of cycles (History of Fatigue, n.d.)

In 1938 Modern bonded wire resistant which called strain gauge invented by Edward E. Simmons & Arthur C. Ruge independently.

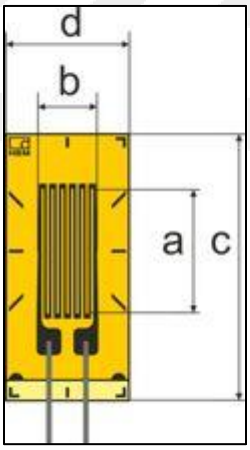

Figure 5.4 Strain gauge (LY Linear Strain Gauges, n.d.)

In 1945 – M. A. Miner makes well known a damage model which was first proposed by A. Palmgren in 1924. This model based on linear damage accumulation where fatigue failure occurs at different stress amplitudes. Later than this model is known in literature as Palmgren-Miner’s rule (Figure 5.5).

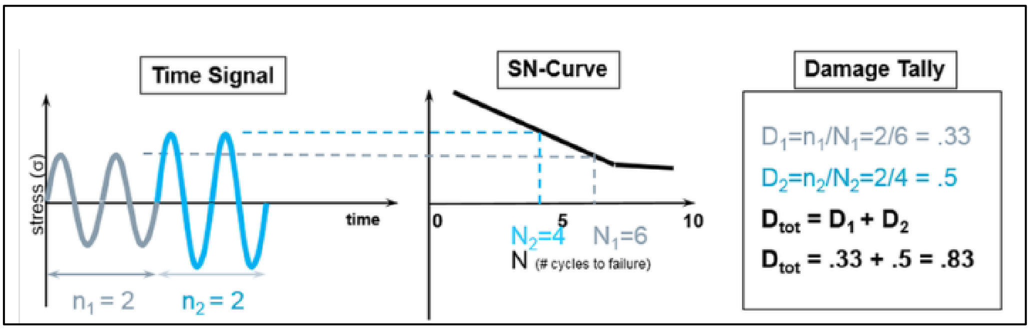

Figure 5.5 Miner's Rule and damage tally (Calculating damage with Miner’s Rule, n.d.)

Manson-Coffin separated low cycle fatigue behavior plastic region of materials where strain exceeds over fatigue limit in 1954.

Tatsuo Endo, a Japanese engineer develops most famous complex load history stress amplitude classification method which is called Rainflow Counting Algorithm. And first Rainflow Counting standard ASTM E1049-85 was published in 1986. It is said that Endo get inspired Pagoda (Figure 5.6) shape which is common in eastern architecture.

Figure 5.6 Pagoda picture (Pagoda, n.d.)

Typcal fatigue failure crack photo is showned in Figure 5.7.

Figure 5.7 Wheel fatigue failure picture (Personal archive, 2020)

5.2 Fatigue Life Predictions

Under cyclic loads, machine elements suffer damage over time, even at stresses that are considerably lower than their yield strength. Fatigue life of the materials is indicated by the number of cycles at which the crack begins. Fatigue life is divided into two according to the order of N cycle number, with N repeat numbers of loads affecting the machine element. If the number of cycles is greater than 1 and less than 1,000, it is called low cycle fatigue, if it is greater than 1,000, it is called high cycle fatigue. There are three basic approaches for estimating the fatigue life of the parts. These are strain - life, stress - life and fracture mechanics approach (Aksoy, 2014).

5.2.1 Strain – Life Prediction

The strain-life approach is used for life prediction in low cycle fatigue. It is based on the association of local strain values with the onset of cracks in loads where the part is subjected to plastic strain. In this approach, the total strain value (ε) should be evaluated separately as the elastic strain (ε_e) and plastic strain (ε_p) values. Hooke's law

(Formula 5.1) is used to find elastic strain, Ramberg Osgood equation (Formula 5.2) is used to find plastic strain (Aksoy, 2014).

$$\varepsilon_{\mathrm{e}}=\frac{\sigma}{E} \tag{5.1}$$

Where E is equal to Young Modulus and σ is stress.

$$\varepsilon_{\mathrm{p}}=\left(\frac{\sigma}{K}\right)^{\frac{1}{n}} \tag{5.2}$$

In the Ramberg Osgood equation in Formula 5.2, the K material constant, n is the relation constant between elastic and plastic strain.

Elastic strain - number of cycles and plastic strain - cycle number relations are shown with Formula 3.3 and Formula 3.4. Total strain – number of cycles is given Formula 5.5. Fatigue life prediction is given Formula 5.6.

$$\frac{\Delta\varepsilon_{\mathrm{e}}}{2}=\frac{\sigma'_{\mathrm{F}}}{E}(2N_{\mathrm{f}})^{b} \tag{5.3}$$

$$\frac{\Delta\varepsilon_{\mathrm{p}}}{2}=\varepsilon'_{\mathrm{f}}(2N_{\mathrm{f}})^{c} \tag{5.4}$$

$$\frac{\Delta\varepsilon}{2}=\frac{\Delta\varepsilon_{\mathrm{e}}}{2}+\frac{\Delta\varepsilon_{\mathrm{p}}}{2} \tag{5.5}$$

$$\frac{\Delta\varepsilon}{2}=\frac{\sigma'_{\mathrm{F}}}{E}(2N_{\mathrm{f}})^{b}+\varepsilon'_{\mathrm{F}}(2N_{\mathrm{f}})^{c} \tag{5.6}$$

Here ε'_F fatigue ductility coefficient, $\frac{\sigma'_F}{E}$ fatigue strength coefficient, c fatigue ductility constant, b fatigue strength constant, $2N_f$ fatigue life cycle.

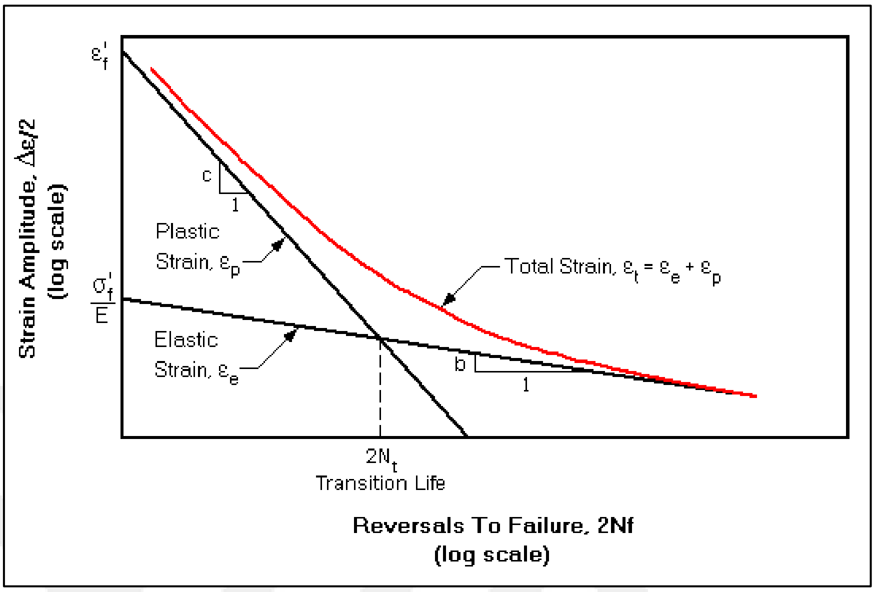

Figure 5.8 Strain fatigue life relationship (Budynas & Nisbett, 2006)

The relationship between fatigue life and strain amplitude is shown in Figure 5.8 depending on the total amount of elongation.

5.2.2 Linear Elastic Fracture Mechanics Approach

When the fatigue crack is examined in micro size, the first stage of the crack occurs due to dislocations occurring between the particles. In the second stage where the crack begins to propagate, the crack reaches the size that can be examined with an electron microscope. In the third stage, crack propagation occurs when the stress intensity factor (KI) at the crack tip equals the fracture toughness (KIc) of the material.

$$K_I = \beta\, \sigma\sqrt{\pi a} \tag{5.7}$$

β= Load density modification factor

a= Crack length [m]

σ = Stress [MPa]

K_I= Stress intensity factor [MPa$\sqrt{m}$]

In the graph in Figure 5.9, the stages of crack propagation, progression and imbalance are shown depending on the factor of breaking intensity.

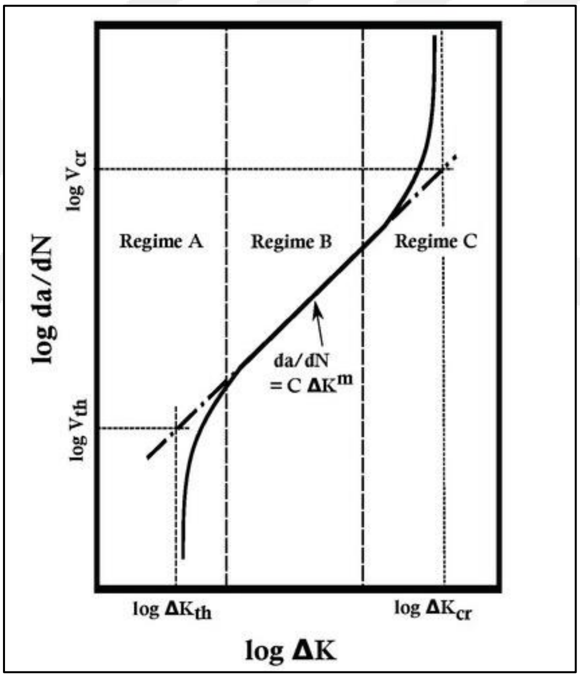

Figure 5.9 Paris law (Budynas & Nisbett, 2006)

5.2.3 Stress – Life Prediction

This approach addresses the method of determining the number of cycles the material is damaged under repeated loads. If more than 1,000 cycles are required for the part to suffer from fatigue damage, the stress-life approach is used.

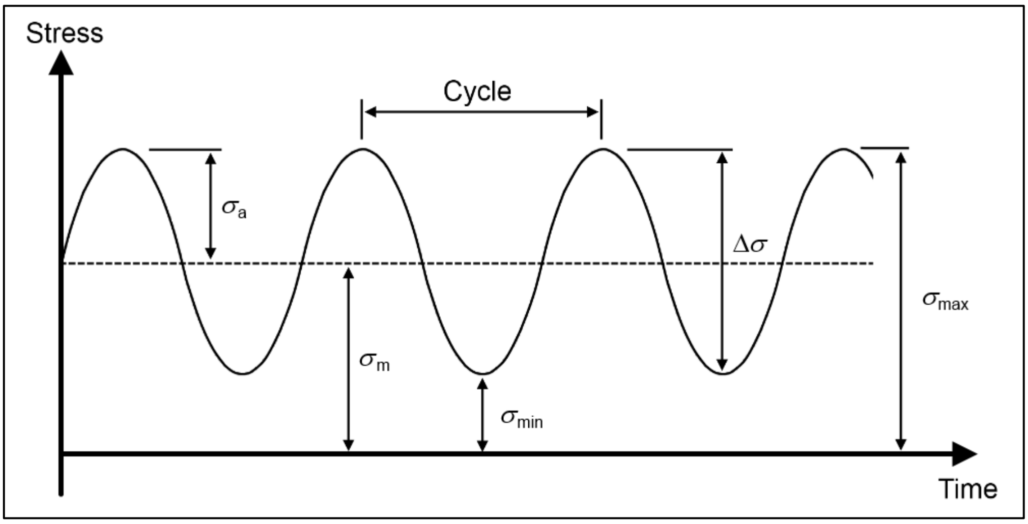

Figure 5.10 Periodic loading graph (Comsol, 2018)

$$\frac{\Delta\varepsilon}{2} = \frac{\sigma'_F}{E}(2N_f)^b + \varepsilon'_F(2N_f)^c$$

Figure 5.10 shows the time-dependent variation of the stress that causes fatigue. The stress varies between maximum (σ_{max}) and minimum (σ_{min}) throughout the load cycle. In fatigue damage calculations, the variation of stress can also be demonstrated using stress amplitude (σ_a) and average stress (σ_m). Also, stress ratio (R) and amplitude ratio (A) are frequently used to describe a stress cycle.

$$\sigma_a = \frac{\Delta\sigma}{2} = \frac{\sigma_{max} - \sigma_{min}}{2} \tag{5.8}$$

$$\sigma_m = \frac{\sigma_{max} + \sigma_{min}}{2} \tag{5.9}$$

$$R = \frac{\sigma_{min}}{\sigma_{max}} \tag{5.10}$$

$$R = \frac{\sigma_a}{\sigma_m} \tag{5.11}$$

$$\sigma_a = \frac{\Delta\sigma}{2} = \frac{\sigma_{max}}{2}(1 - R) \tag{5.12}$$

$$\sigma_m = \frac{\sigma_{max}}{2}(1 + R) \tag{5.13}$$

$$R = \frac{1 - A}{1 + A} \tag{5.14}$$

$$A = \frac{1 - R}{1 + R} \tag{5.15}$$

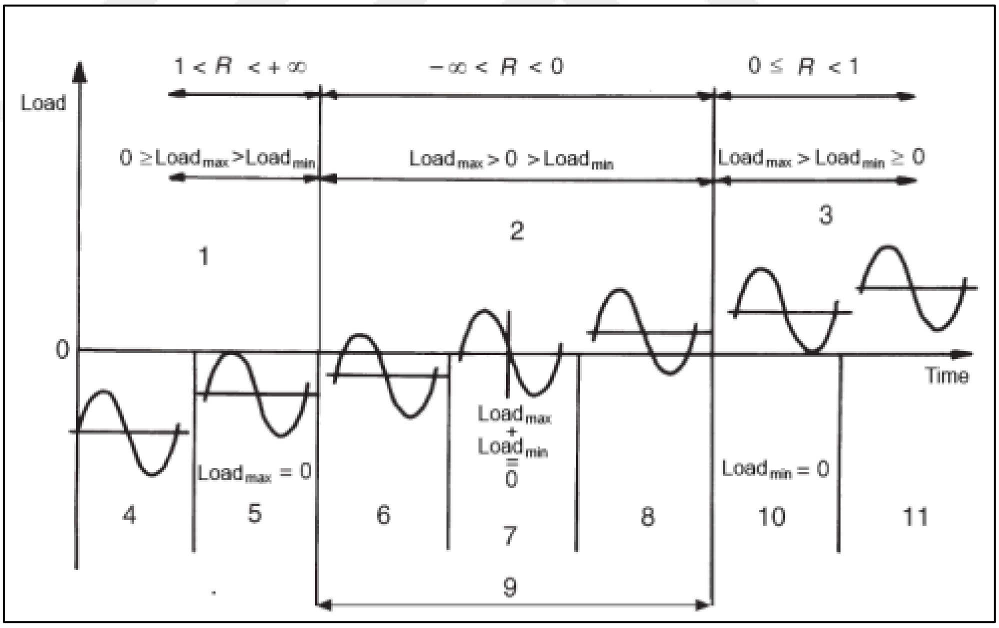

Figure 5.11 R ratio effect (Marques, 2013)

Figure 5.11 shows the R values and the types of the fatigue stress cycle according to different average stresses. Fatigue stress for the R> 1 condition is in the direction of compression. For the case of 0 <R <1, the fatigue stress acts as the tensile stress on the part. For R = -1, the maximum and minimum values in the stress cycle are equal to each other as absolute values and named full reverse cycle. For this reason, the average fatigue stress value on the part is 0.

5.3 Rainflow Cycle Counting Method

Figure 5.12 shows fatigue test condition and field usage condition load distribution comparison. It is easy to evaluate test condition load distribution by using literature knowledge. When the load history becomes more complicated it is not easy to determinate fatigue damage anymore. These values have to classified. Rainflow cycle counting method is invented to classify load history data to mean stress and amplitude.

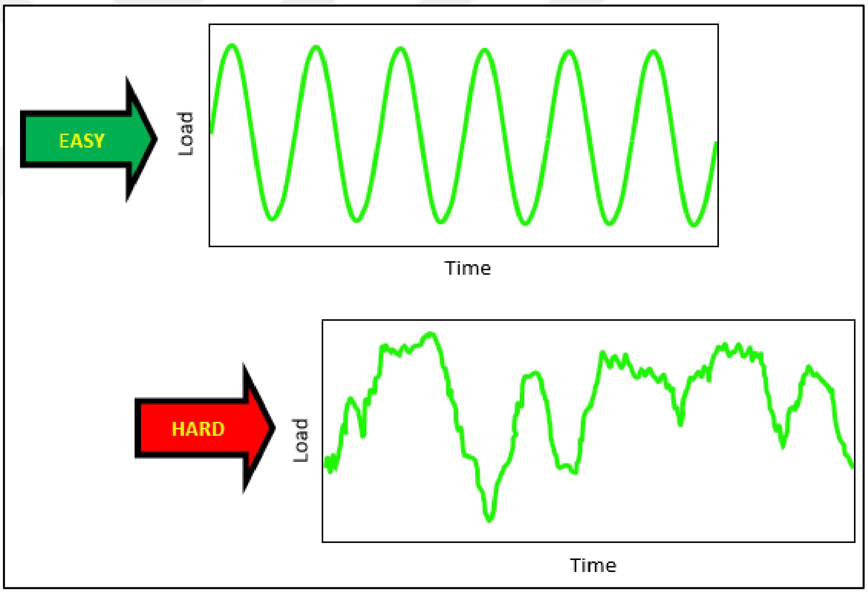

Figure 5.12 Test and field usage loading history chart (Rainflow Counting, n.d.)

In 1967, Tatsuo Endo, suggested a method called “Rainflow Cycle Counting” to classify stress amplitude and mean values any load-time history into its constituent fatigue cycles.

Rainflow algorithm steps are as below:

The function counts cycles by considering a moving reference point which is defined "Z" and a moving ordered three-point subset with these values. The first and second points are denoted Y. The second and third points are called X. In both X and Y, the points are sorted from earlier to later in time, but are not necessarily consecutive in the reversal sequence. The range of X, called by r(X), is the absolute value of the difference between the amplitude of the first point and the amplitude of the second point. The definition of r(Y) is similarly. Figure 5.13 shows Rainflow Cycle Counting algorithm schematic drawing (Rainflow, n.d.).

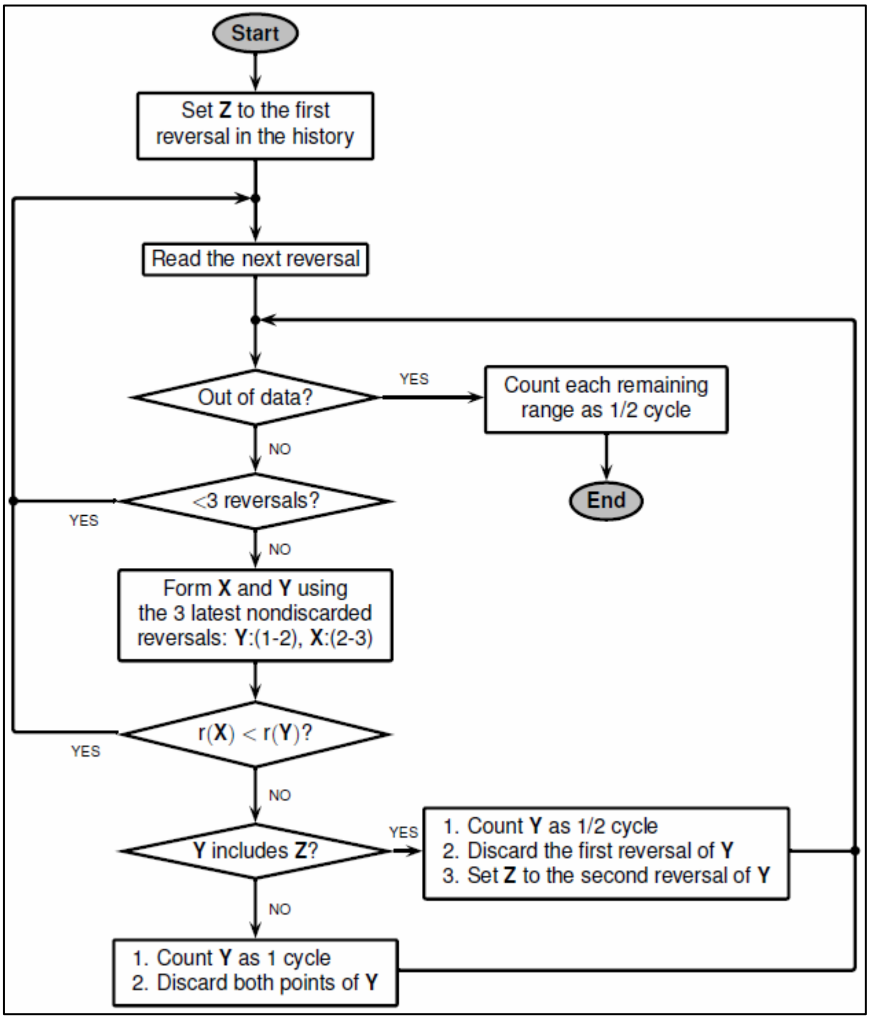

Figure 5.13 Rainflow cycle counting algorithm (Rainflow, n.d.)

At the end, the algorithm stores the different cycles, half cycles and tabulates their amplitudes, their means. This information will be used for wheel biaxial fatigue test machine comparison procedure. Typical output of Rainflow Cycle Counting method range and mean values showed in Figure 5.14.

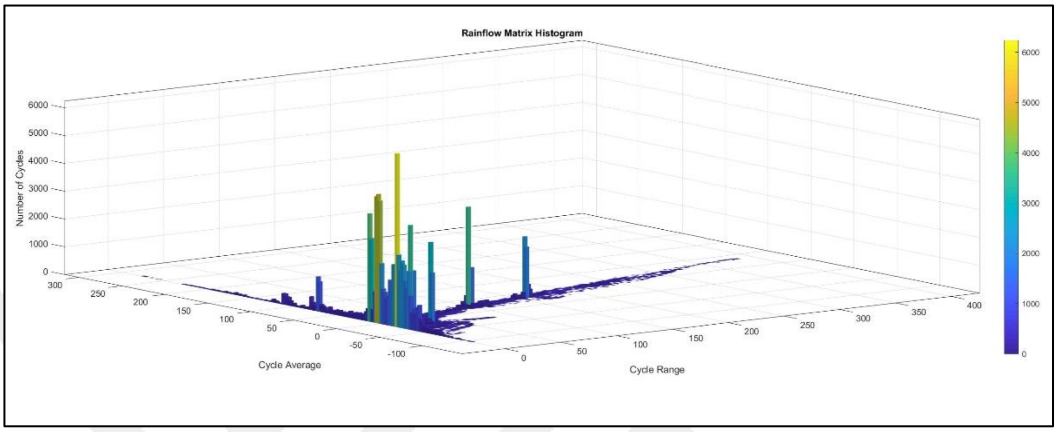

Figure 5.14 Rainflow cycle counting solution matrix graph

In 1986, the first ASTM Rainflow Counting standard, E1049-85, was officially published.

In this study a software was created by using LabView 2015 to classify strain-stress data during wheel fatigue tests according to ASTM E 1049-85. Classified test data will be used in further chapters to compare dynamic bench check by stress analysis for biaxial test machines.

CHAPTER SIX
DYNAMIC STRAIN MEASUREMENT STUDY

6.1 Strain

Strain is the mathematical term that refers to how much a material under load changes its shape compared to the situation before the load is applied. As used herein, shape change does not refer to a formal change, but rather to a quantitative unit elongation in shape.

Strains occur on the wheel during various fatigue tests applied to commercial vehicles. These strains that occur during testing and machine verification study will be done further chapters.

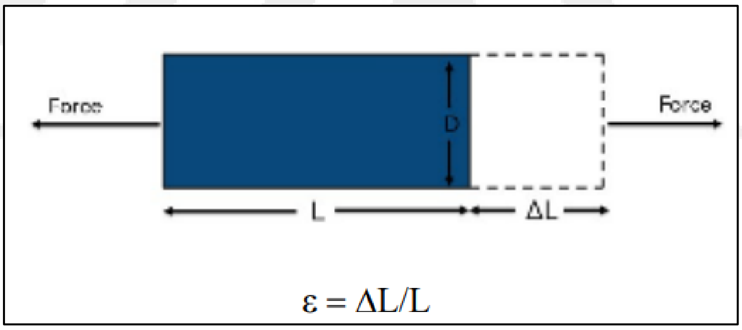

Figure 6.1 Strain figure (Poyraz, Akkan, & Şahin, 2019)

6.2 Strain Gauge

Strain gauge is a device used for measuring strain on a material. It was invented by Edward E. Simmons & Arthur C. Ruge in 1938. As a basic working principle, it is based on the perception of the change in unit elongation as an electrical signal by using the resistance change. The perceived signal is the strain gauge resistance change in the mini volt range. A Wheatstone bridge is required to make the measurement. There are 4 resistors on the Wheatstone bridge, while the bridge is fed with a warning voltage, on the other hand, resistance changes due to deformation are measured. 4 resistance or 4 strain gauge is required for full bridge measurement. There are also measurement types called half and quarter bridges. In such cases, there are 1 or 2 strain gauges. Missing resistors must be completed by external bridge completion resistors. Bridge completion resistors must be of high accuracy and precision. The schematic drawing of the Wheatstone bridge consisting of a quarter bridge is shown in Figure 6.2.

The strain gauge is rigidly adhered on the piece to be measured with the help of special adhesives. Before applying the bonding process, the surface of the part where the strain gauge will be applied should be polished very well and this polished area should be wiped with chemicals such as alcohol and cleaned from small dust.

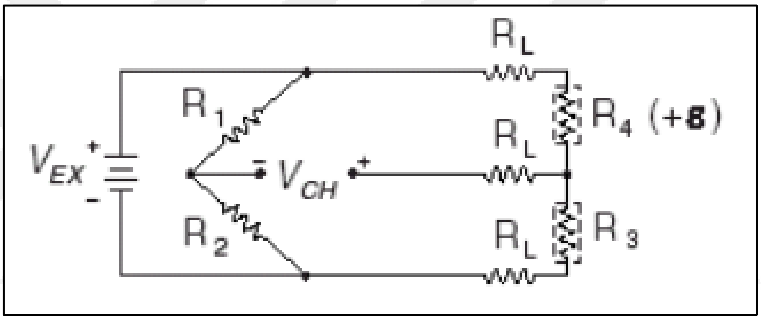

Figure 6.2 Quarter bridge Wheatstone bridge schematic drawing (Gül, 2015)

6.3 Measurement Wheel Preparation

In chapter 4 dynamic bench check by stress analysis method was given. According this information 6 strain gauges applied to the commercial wheel. Measurement wheel pictures shared in Figure 6.3, Figure 6.4 and Figure 6.5.

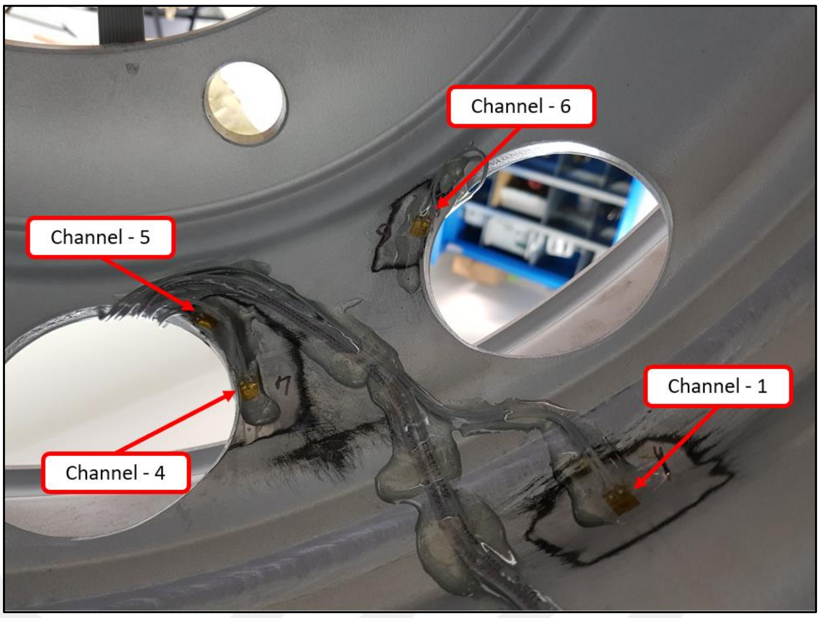

Figure 6.3 Measurement wheel channel strain gauge no 1, 4, 5, 6 picture (Personal archive, 2020)

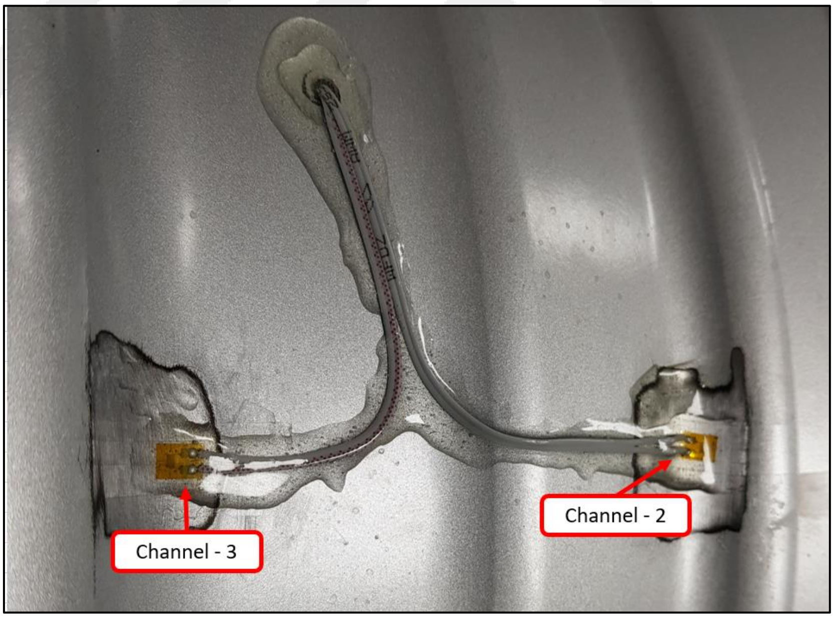

Figure 6.4 Measurement wheel channel strain gauge no 2, 3 picture (Personal archive, 2020)

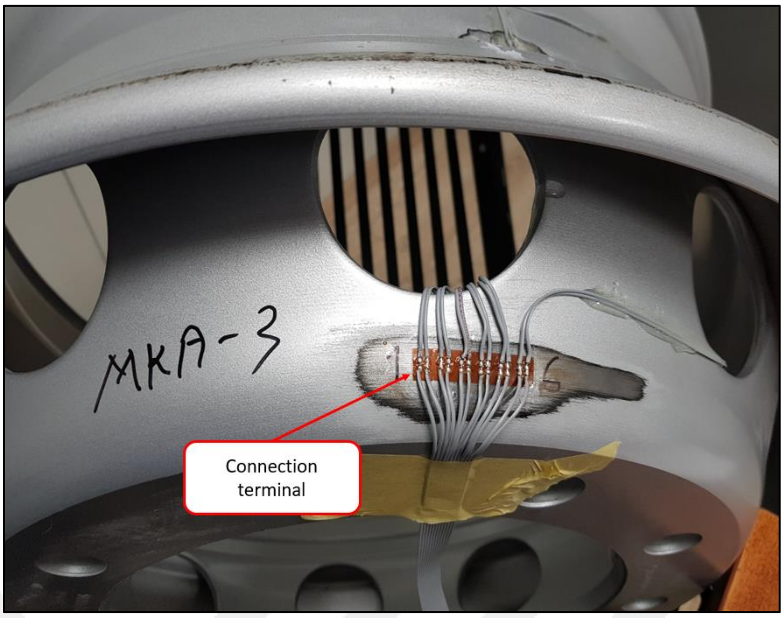

Figure 6.5 Measurement wheel connection terminal picture (Personal archive, 2020)

6.4 Data Acquisition Device

Embedded real time data acquisition program is created with using LabView 2015 software. The system sample rate is up to 10kHz. Strain values are recorded to NI cRIO-9025 nonvolatile memory during measurement. Data acquisition system shared in Figure 6.6.

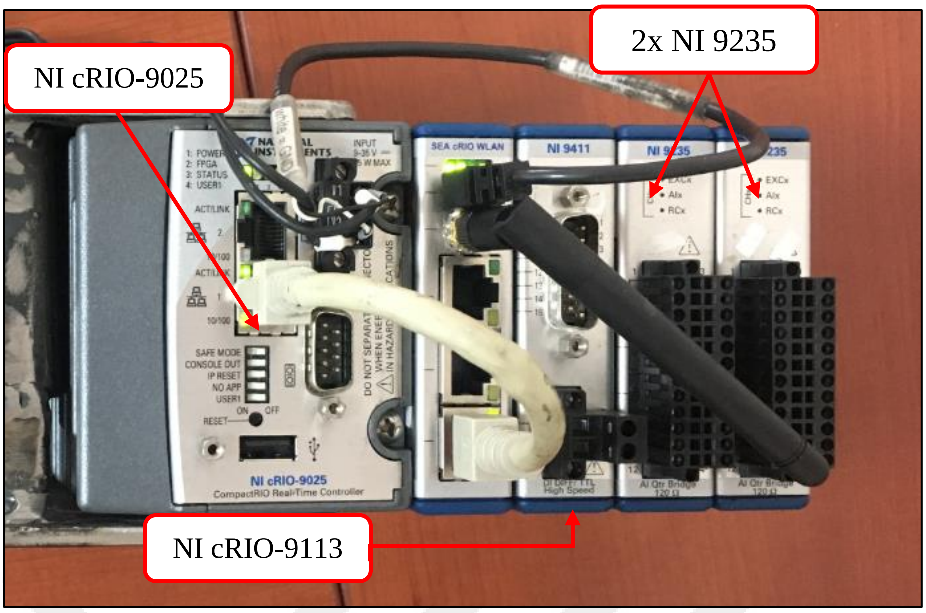

Figure 6.6 National Instruments data acquisition device picture (Personal archive, 2020)

NI cRIO-9025 Intelligent Real-Time Embedded Controller for CompactRIO is an embedded real-time controller ideal for advanced control and measurement applications. The controller has 800Mhz CPU, 512MB DRAM and 4 GB nonvolatile memory storage.

NI cRIO-9113 Reconfigurable Embedded Chassis is rugged FPGA chassis that you can add C series I/O modules to your distributed control and measurement applications. Chassis has 4 Slots, Virtex-5 LX50 FPGA, 28,800 number of flip-flops, 48 number of DSP48 slices 25x18 multipliers and 1,728kbits embedded block RAM.

NI 9235 C series 8 Channel Quarter bridge 120 Ω strain gauge module measures dynamic strain on all channels simultaneously, allowing for synchronized, high-speed measurements.

6.5 Strain Measurement

In this study, only data for biaxial fatigue tests from fatigue tests of heavy commercial vehicle wheels will be collected and examined. Data acquisition details are shared in Table 6.1.

Table 6.1 Data acquisition details

Test Bench Code	Location	Sample Rate [Hz]	DAQ Duration	Chanel Quantity
JAN-1	Maxion Wheels Jantaş / Türkiye	2,000	1 Eurocycle / 65km	6
JAN-2	Maxion Wheels Jantaş / Türkiye	2,000	1 Eurocycle / 65km	6
REF	Outsource Test Facility	2,000	1 Eurocycle / 65km	6

An example representation of the data consisting of 1 Eurocycle for channel 1 is shared in Figure 6.7. The number of data collected for a single channel, consisting of 1 Eurocycle which is approximately 65km, is 4,760,000. Since there are 6 channels in total, the total number of data is 28,560,000 for 1 Eurocycle measurement.

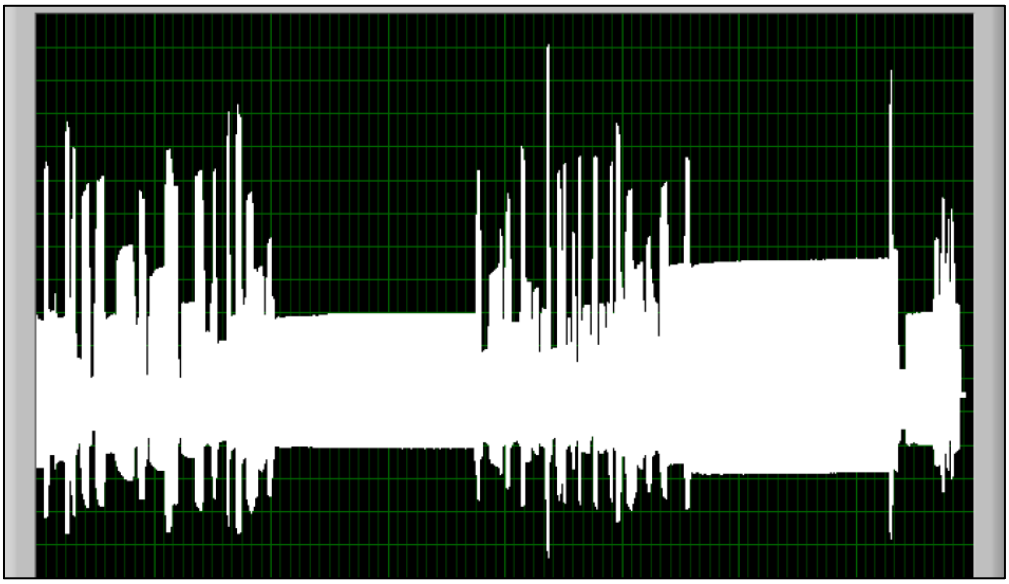

Figure 6.7 Channel 1 Eurocycle measurement result example

The collected data for each channel is 4,760,000. A special program and method are needed to evaluate data of this size. A special software is developed by using LabVIEW 2015 for the analysis of large amounts of data. For the analysis of these data, firstly collected strain data is converted to stress, then rainflow cycle counting method is applied and finally mean stress correction models are applied for fatigue damage calculation.

CHAPTER SEVEN
RESULTS

In this section strain-stress measurement results will be shared. According collected strain-stress values rainflow cycle counting method will be applied. Then RFS (Required Fatigue Strength) values will be calculated with respect to E.U.W.A. 3.29 check and calibration procedures for fatigue test benches of wheel.

7.1 Strain Measurement Results

The NI cRIO 9025 measures strain values in mV unit. mV values converted to strain values given Equation 7.1.

$$\varepsilon = \frac{-4 * \left(\frac{Vsg - Vinit}{Vex}\right)}{GF * \left(1 + 2 * \left(\frac{Vsg - Vinit}{Vex}\right)\right)} * \left(1 + \frac{RL}{Rg}\right) \tag{7.1}$$

Where;

ε: Strain

Vsg: Measured voltage [mV]

Vinit: Unstrained voltage of strain gauge [mV]

Vex: Excitation voltage [mV]

GF: The gauge factor of strain gauge

RL: Lead resistance [ohm]

Rg: Nominal strain gauge resistance [ohm]

Three different wheel biaxial test machine measured. Their channel 1 strain measurement results are given in Figure 7.1, Figure 7.2, Figure 7.3. Channel 2 to 6 values are given in Appendices 1 to Appendices 5.

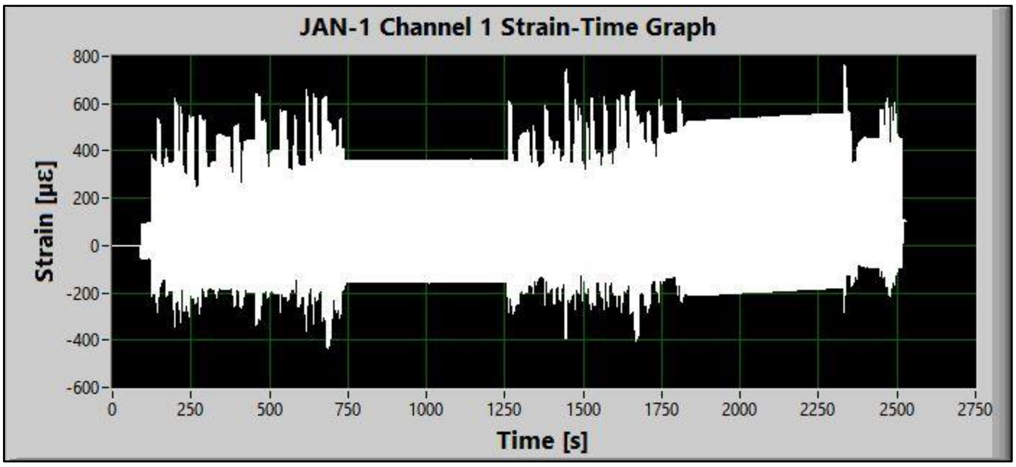

Figure 7.1 JAN-1 Channel-1 strain-time graph

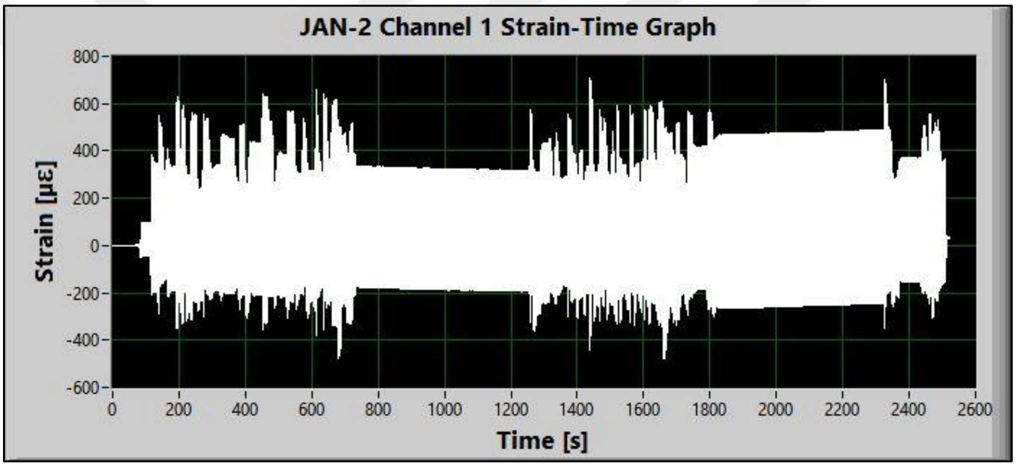

Figure 7.2 JAN-2 Channel-1 strain-time graph

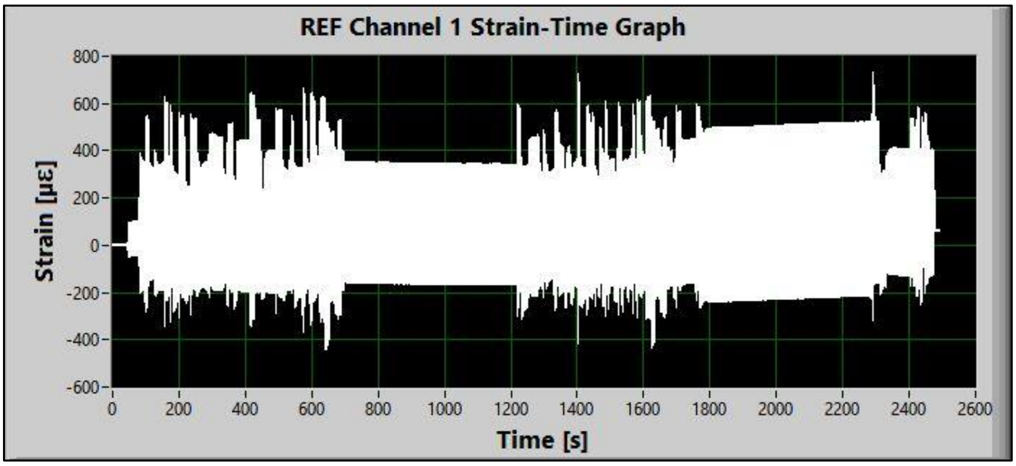

Figure 7.3 REF Channel-1 strain-time graph

7.2 Rainflow Cycle Counting Results

Before RFS calculation, measured strain values have to convert stress values according to the E.U.W.A 3.29 standard. Strain stress conversion is done given equation below. Young modulus for steel material is chosen 210,000MPa.

$$\sigma = E * \varepsilon \tag{7.2}$$

Where:

σ: Stress [MPa]
E: Young Modulus [GPa]
ε: Strain

For each wheel biaxial fatigue test machine measurement data rainflow cycle counting study is done by special software which is created for this thesis study. For each wheel biaxial fatigue test machines channel 1 stress Rainflow Cycle Counting matrix shared Figure 7.4, Figure 7.5 and Figure 7.6. Channel 2 to 6 results are given Appendices 6 to Appendices 10.

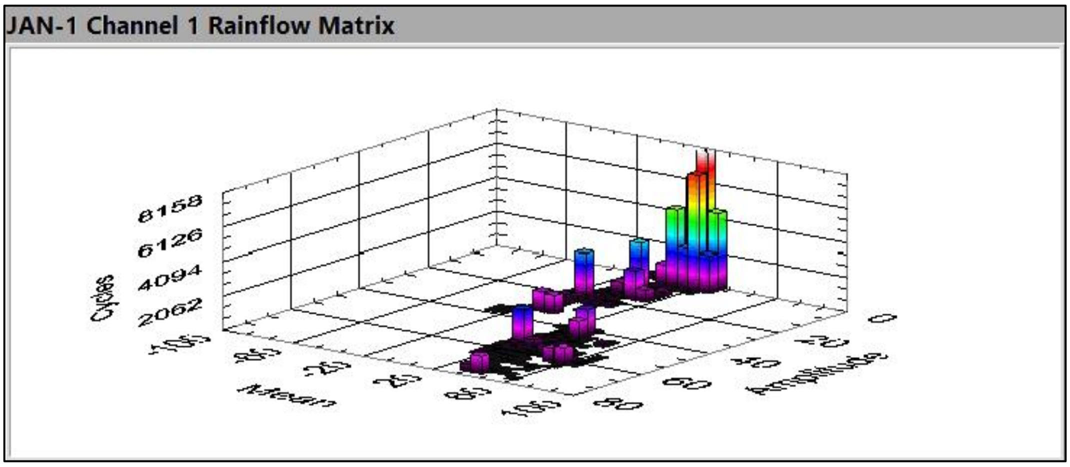

Figure 7.4 JAN-1 Channel-1 rainflow solution matrix

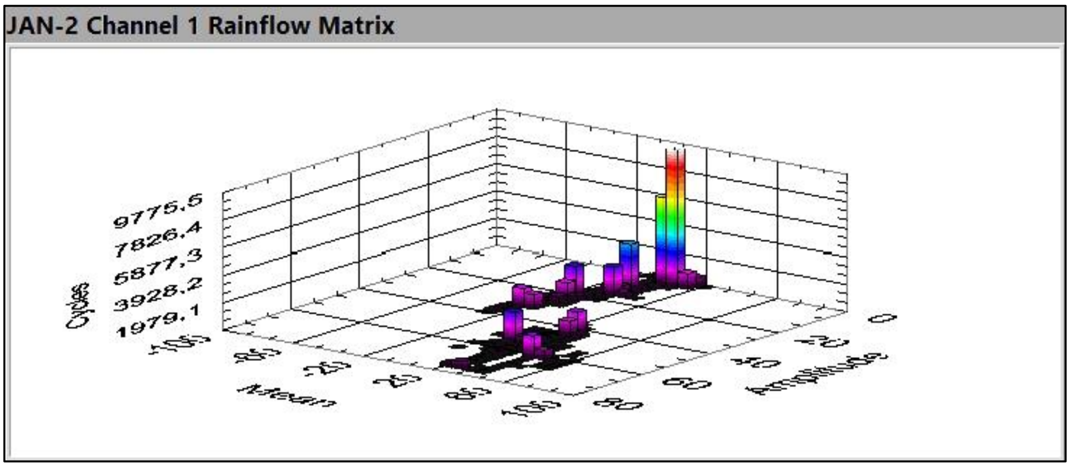

Figure 7.5 JAN-2 Channel-1 rainflow solution matrix

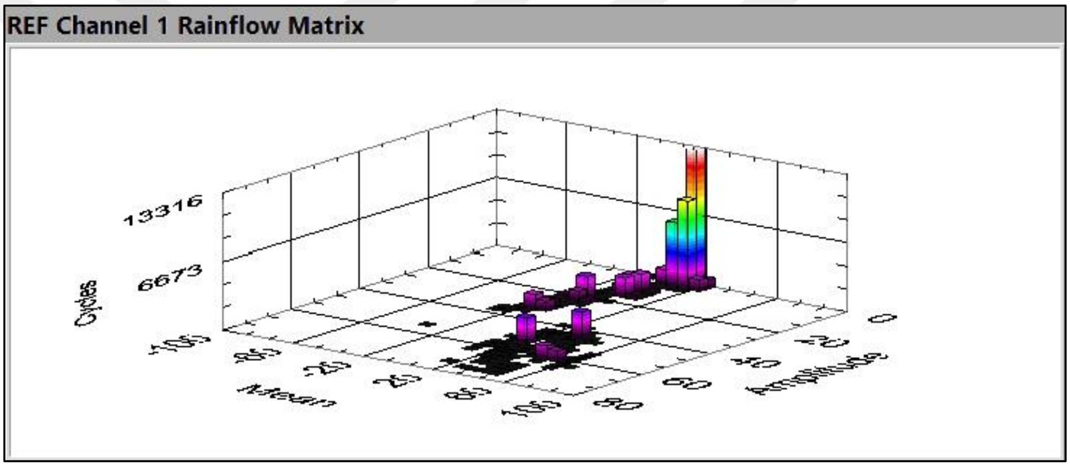

Figure 7.6 REF Channel-1 rainflow solution matrix

7.3 RFS Value Calculation Results

Required Fatigue Strength nomenclature defined in E.U.W.A. 3.29 Check and calibration procedures for fatigue test benches of wheel standard. This value can be determined only iterative way by using rainflow cycle counted stress data. Thus special software created for calculation of Required Fatigue Strength. For each different wheel biaxial test machine measured data is evaluated and calculated RFS value comparsion graphs are given following figures.

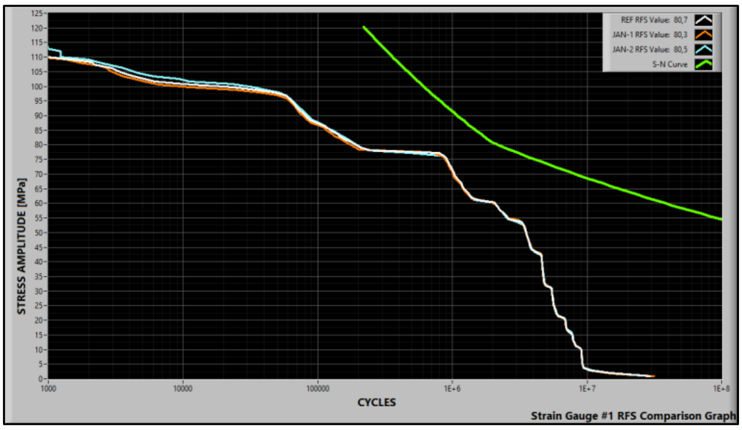

Figure 7.7 Channel-1 RFS Comparsion graph

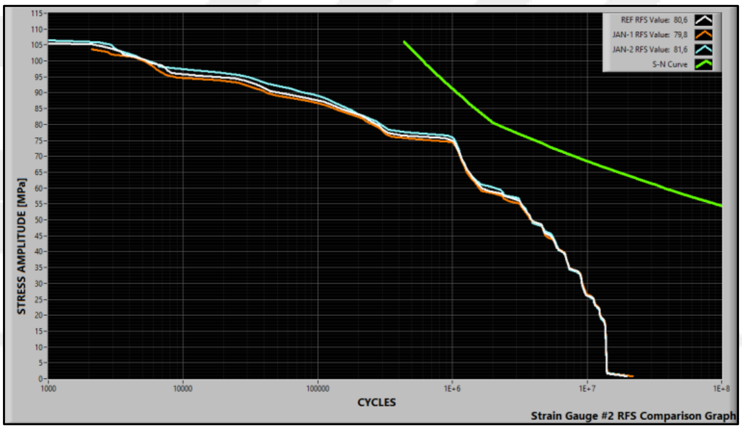

Figure 7.8 Channel-2 RFS Comparsion graph

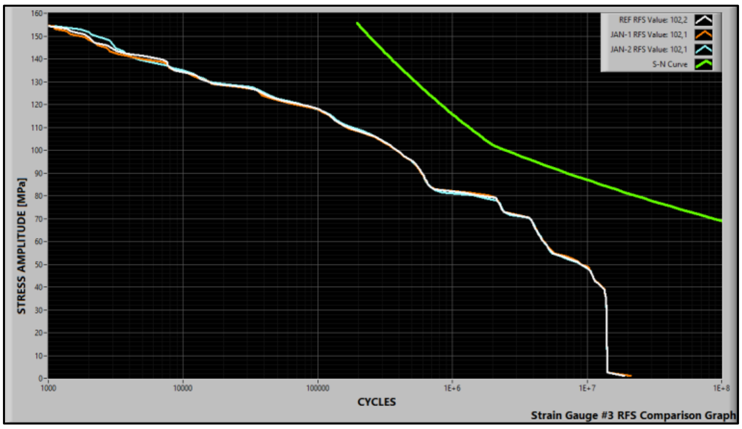

Figure 7.9 Channel-3 RFS Comparsion graph

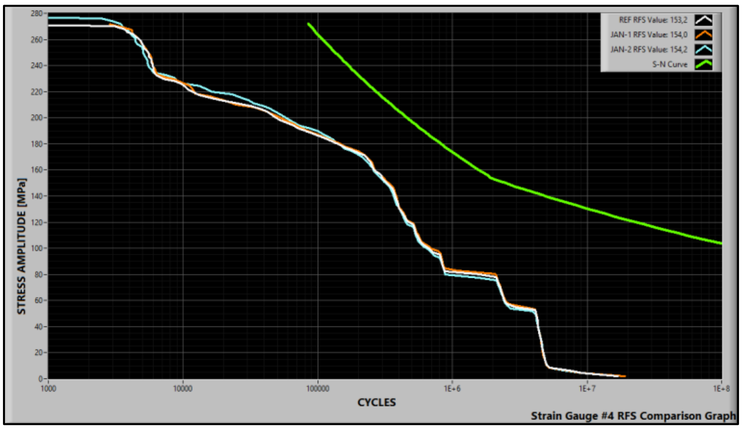

Figure 7.10 Channel-4 RFS Comparsion graph

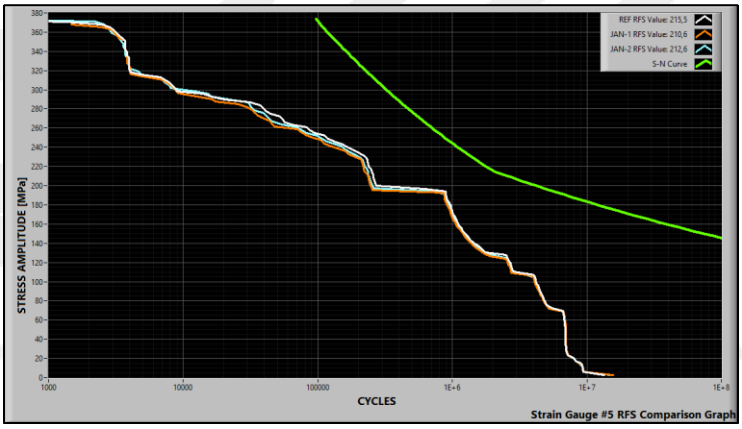

Figure 7.11 Channel-5 RFS Comparsion graph

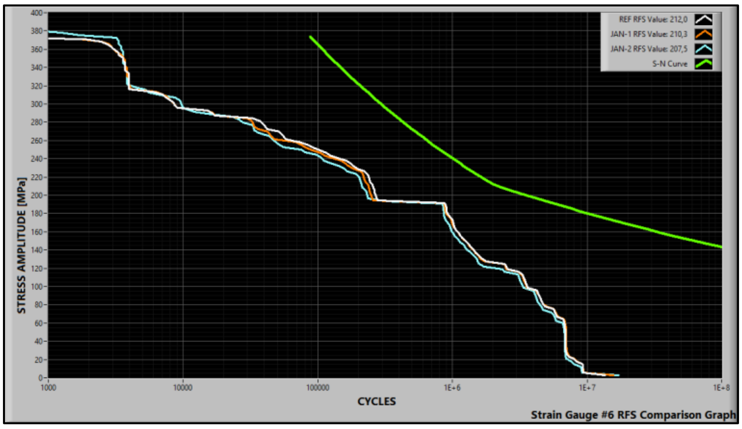

Figure 7.12 Channel-6 RFS Comparsion graph

Table 7.1 RFS Results comparsion table

	RFS Value [MPa]			%Deviation	
	JAN-1	JAN-2	REF	JAN-1	JAN-2
Channel 1	80.3	80.5	80.7	0.5	0.2
Channel 2	79.8	81.6	80.6	1.0	-1.2
Channel 3	102.1	102.1	102.2	0.1	0.1
Channel 4	154	154.2	153.2	-0.5	-0.7
Channel 5	210.6	212.6	215.5	2.3	1.3
Channel 6	210.3	207.5	212	0.8	2.1

Measurement wheel measured at three different wheel biaxial fatigue test machine and RFS values calculated. RFS results are given Table 7.1. According to E.U.W.A. 3.29 RFS value deviation has to be under ±%5. When JAN-1 and JAN-2 machines RFS deviation comprised to REF machine for all strain gauge locations this value fitted to defined tolerance. Thus, these results show Jantaş's all two wheel biaxial fatigue test machine equivalent to Reference Machine.

CHAPTER EIGHT
CONCLUSION

In this study, the manufacturing methods of steel commercial vehicle wheels were examined. Firstly, international standards used in determining the fatigue life of steel commercial vehicle wheels and the test methods described by these standards were emphasized. In addition, the verification procedures of the test machines were examined.

In the second stage, information was given about strain gauges and explanations were made about data collection methods. In order to perform test machine verification procedures, a measurement wheel with strain gauges was created. Measurements were taken from three different heavy commercial vehicle biaxial test machines. Rainflow cycle counting method is explained and special software for this method has been developed in LabVIEW 2015 program.

The obtained analyzed RFS data was compared with the reference machine, REF machine, whose accuracy is known. RFS value should be within ± 5% according to E.U.W.A 3.29. It has been observed in the measurements that all channels are within this limit. Thus, the accuracy of Maxion Wheels Jantaş biaxial test machines has been proven. This verification study will be repeated once a year to ensure that the relevant test machine works correctly.

This work can be repeated by taking strain measurements on them during the new wheel design studies or the improvement of existing products. Thus, stress values can be obtained newly designed wheels. At the same time, between finite element analysis and fatigue test correlation studies can be conducted with this study in the upcoming years.

REFERENCES

Aksoy, K. O. (2014). *Yedek teker taşıyıcı sisteminin titreşim kaynaklı yorulma analizi.* Master Thesis, İstanbul Teknik Üniversitesi, İstanbul.

Association of European Wheel Manufaturers. (2006, Mayıs). *EUWA ES-3.11 Test Requirements for Truck Steel Wheels.* Retrieved from https://www.euwa.org/wp-content/uploads/2018/05/EUWA-ES-3.11-Test-Requirements-for-Truck-Steel-Wheels..pdf

Association of European Wheel Manufaturers. (2017, June). *EUWA ES-3.23 Biaxial Fatigue Test for Trucks Wheels.* Retrieved from https://www.euwa.org/wp-content/uploads/2018/05/EUWA-ES-3.23-Biaxial-Fatigue-Test-for-Trucks-Wheels-1.pdf

Association of European Wheel Manufaturers. (2017, October). *EUWA ES-3.29 Check and calibration procedures for fatigue test benches of wheel.* Retrieved from https://www.euwa.org/wp-content/uploads/2018/05/EUWA-ES-3.29-CHECK-AND-CALIBRATION-PROCEDURES-FOR-FATIGUE-TEST-BENCHES-OF-WHEEL.pdf

BiAx Wheel Test Technology. (n.d.). Retrieved 23 August, 2020, from https://www.zwarp.fraunhofer.de/en/lbf-biaxial-wheel-hub-fatigue-testing/Introduction.html

Budynas, R. G., & Nisbett, K. J. (2006). *Shigley's mechanical engineering design 8th Edition.* New York: McGraw-Hill.

Calculating damage with Miner's Rule. (n.d.). Retrieved June 28, 2020, from https://community.sw.siemens.com/s/article/calculating-damage-with-miner-s-rule

Carboni, M., Beretta, S., & Finzi, A. (2003). Defects and in-service fatigue life of truck wheels. *Engineering Failure Analysis, (10)*, 45-57.

Ercan, S. (2011). *Ticari taşıtlarda kullanılan jantlarda dinamik işletim yükü altında oluşan yorulma ömrünün bilgisayar destekli belirlenmesi.* Master Thesis, Dokuz Eylül Üniversitesi, İzmir.

Grubisic, V., & Fischer, G. (1983). Automotive wheels, method and procedure for optimal design and testing. *Society of Automotive Engineers [SAE] Technical Paper Series*, 830135.

Gül, E. (2015). *Design and implementation of a wireless telemetry system for a solar race car.* Master Thesis, Dokuz Eylül Üniversitesi, İzmir.

History of Fatigue. (n.d.). Retrieved July 3, 2020, from https://community.sw.siemens.com/s/article/history-of-fatigue

LY Linear Strain Gauges. (n.d.). Retrieved May 24, 2020, from https://www.hbm.com/en/4561/ly-linear-strain-gauges-with-1-measurement-grid/

Marques, J. (2013). *Stress Ratio Effects on the fatigue Properties of Biaxially Loaded Tubular FRP-Specimens – Experimental Study.* Master Thesis, Institute for Aircraft Design and Lightweight Structure Technische Universität Braunschweig, Braunschweig.

Pagoda. (n.d.). Retrieved 4 July, 2020, from https://en.wikipedia.org/wiki/Pagoda

Poyraz, U., Akkan, L. Ö., & Şahin, Y. (2019). Theoretical & Experimental Shape Optimization Of Cantilever Beam by Constrained Optimization Method. *International Congress on Human-Computer Interaction,* 162-166

Rainflow. (n.d.). Retrieved July 4, 2020, from https://www.mathworks.com/help/signal/ref/rainflow.html

Rainflow Counting. (n.d.). Retrieved July 4, 2020, from https://community.sw.siemens.com/s/article/rainflow-counting

Topaç, M. M., Ercan, S., & Kuralay, N. S. (2012). Fatigue life prediction of a heavy vehicle steel wheel under radial loads by using finite element analysis. *Engineering Failure Analysis*, *20*, 67-79.

Versailles rail accident. (n.d.). Retrieved July 4, 2020, from https://en.wikipedia.org/wiki/Versailles_rail_accident

APPENDICES

APPENDIX 1: CHANNEL-2 STRAIN-TIME GRAPH

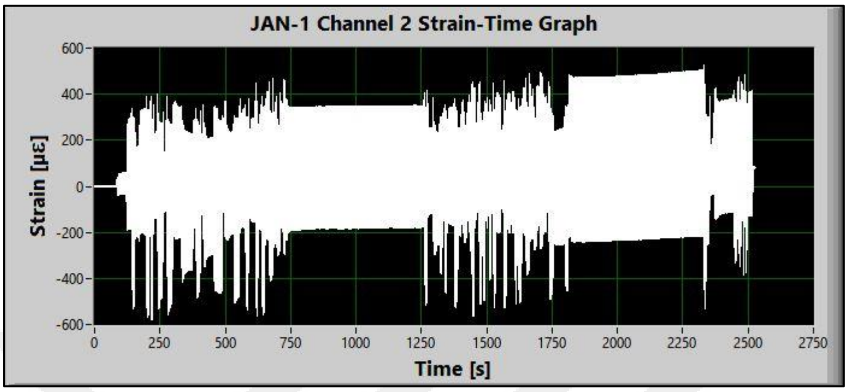

Figure A.1.1 JAN-1 Channel 2 Strain-Time Graph

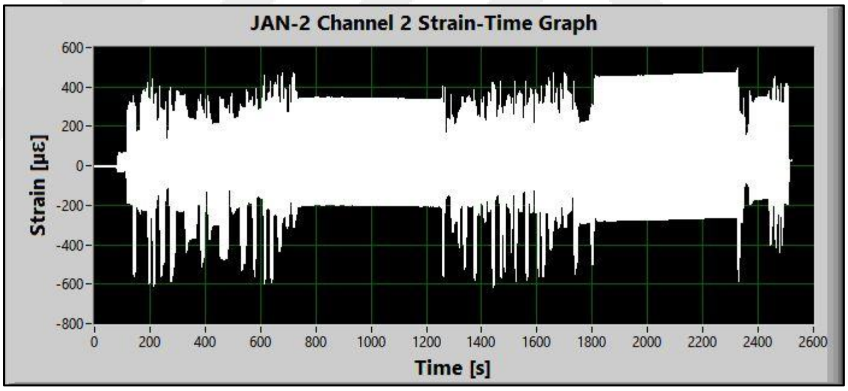

Figure A.1.2 JAN-2 Channel 2 Strain-Time Graph

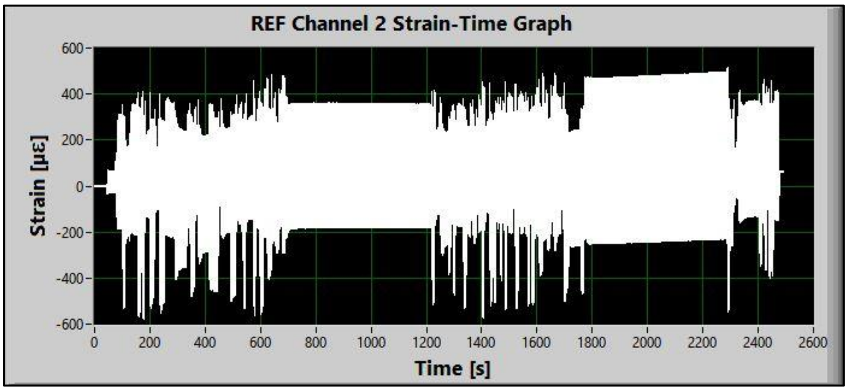

Figure A.1.2 REF Channel 2 Strain-Time Graph

APPENDIX 2: CHANNEL-3 STRAIN-TIME GRAPH

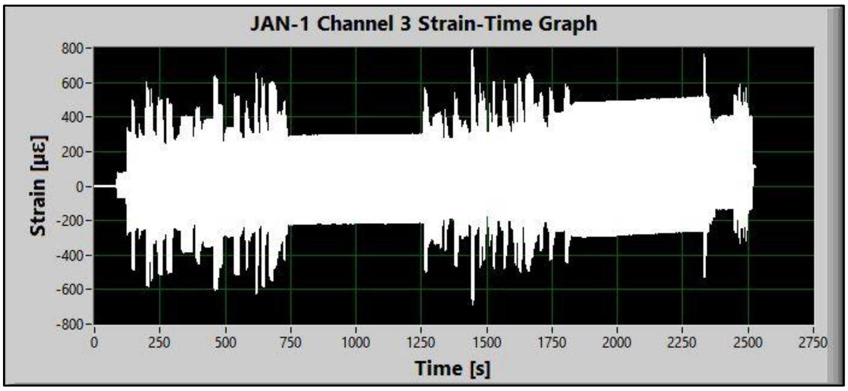

Figure A.2.1 JAN-1 Channel 3 Strain-Time Graph

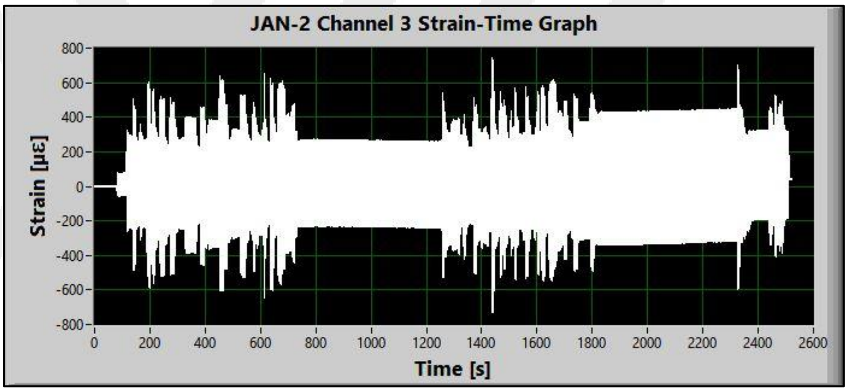

Figure A.2.2 JAN-2 Channel 3 Strain-Time Graph

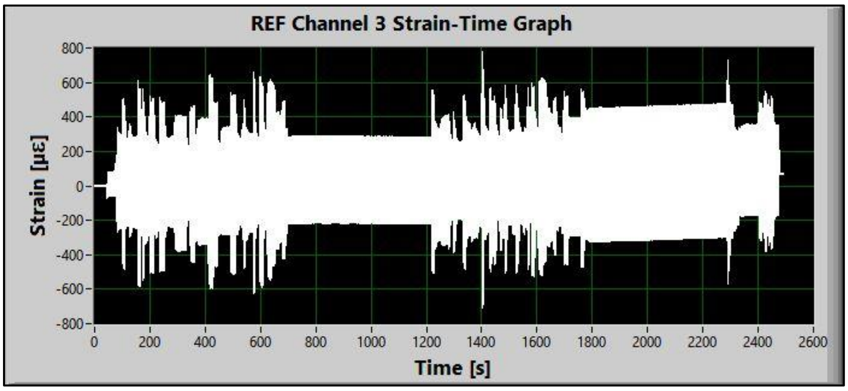

Figure A.2.3 REF Channel 3 Strain-Time Graph

APPENDIX 3: CHANNEL-4 STRAIN-TIME GRAPH

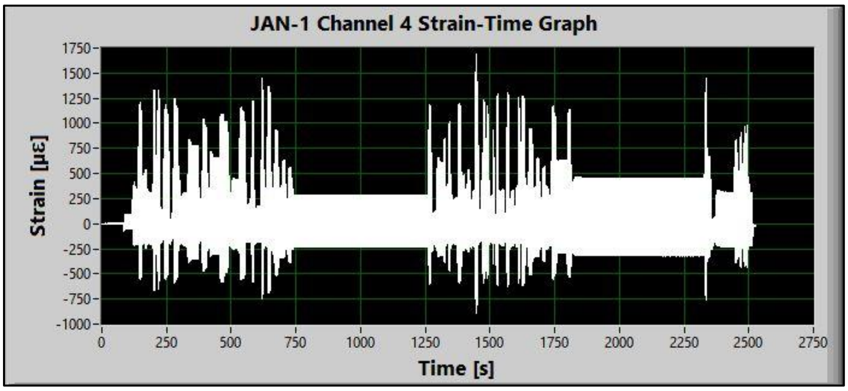

Figure A.3.1 JAN-1 Channel 4 Strain-Time Graph

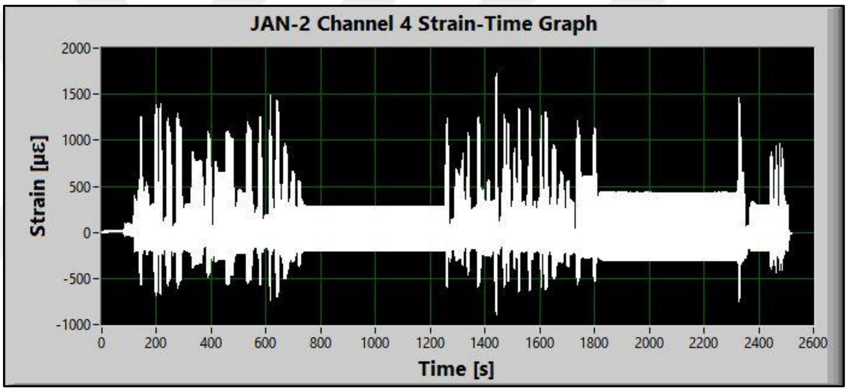

Figure A.3.2 JAN-2 Channel 4 Strain-Time Graph

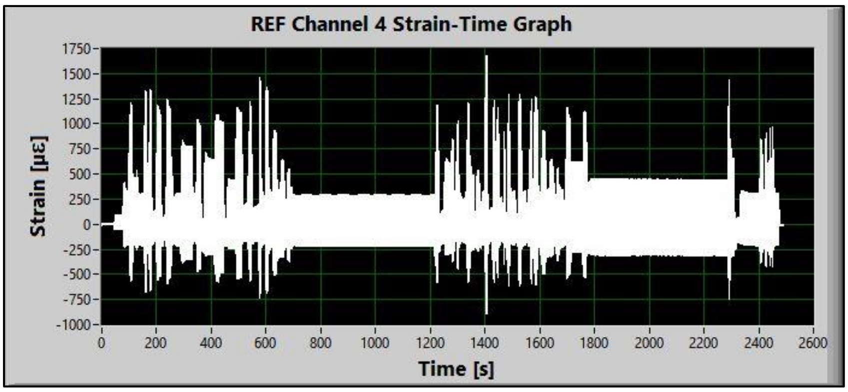

Figure A.3.3 REF Channel 4 Strain-Time Graph

APPENDIX 4: CHANNEL-5 STRAIN-TIME GRAPH

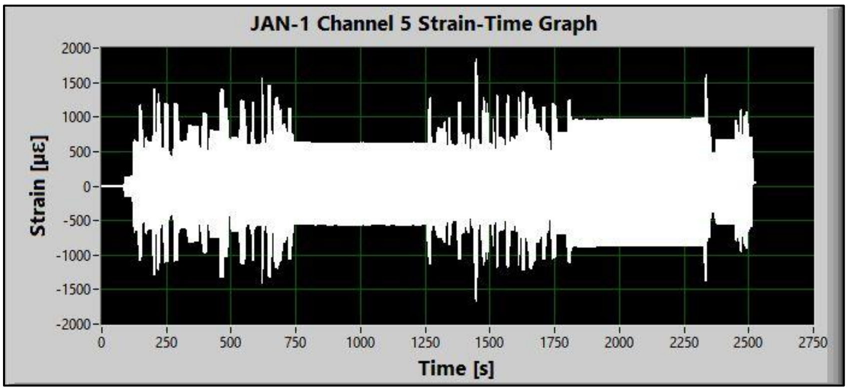

Figure A.4.1 JAN-1 Channel 5 Strain-Time Graph

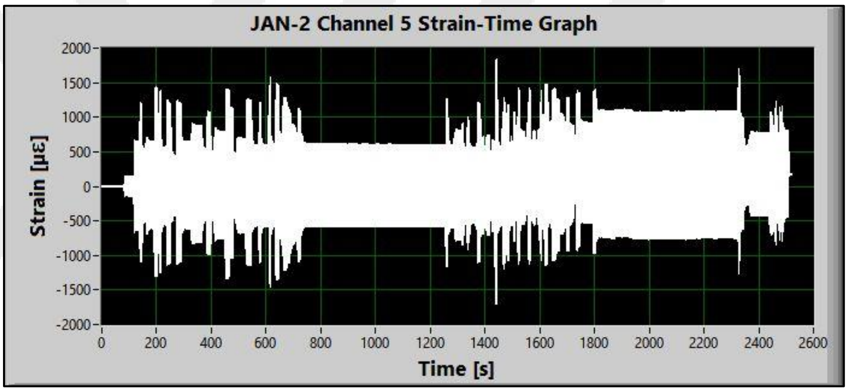

Figure A.4.2 JAN-2 Channel 5 Strain-Time Graph

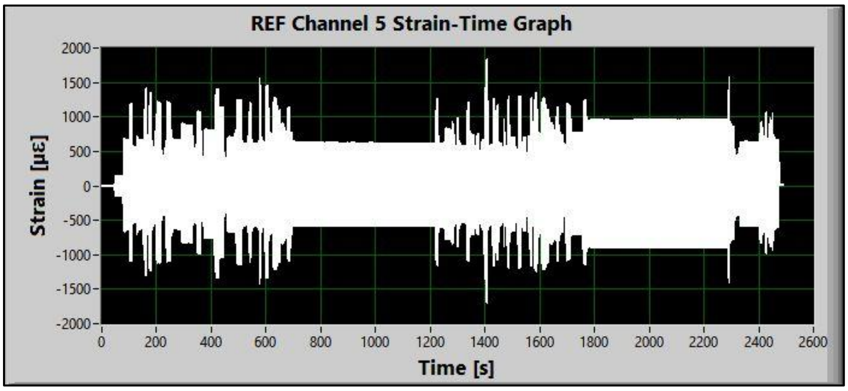

Figure A.4.3 REF Channel 5 Strain-Time Graph

APPENDIX 5: CHANNEL-6 STRAIN-TIME GRAPH

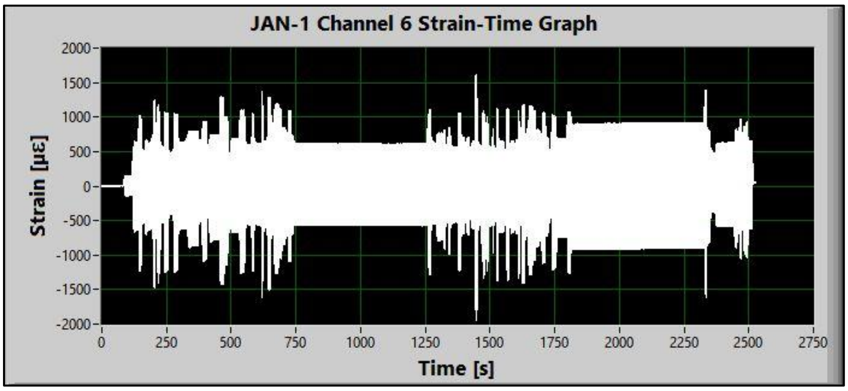

Figure A.5.1 JAN-1 Channel 6 Strain-Time Graph

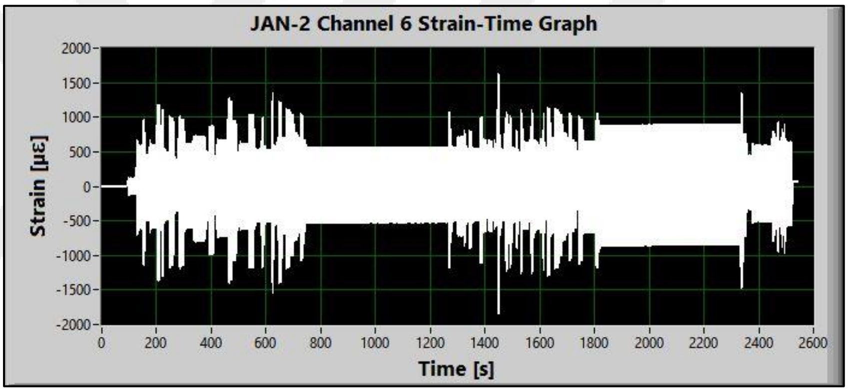

Figure A.5.2 JAN-2 Channel 6 Strain-Time Graph

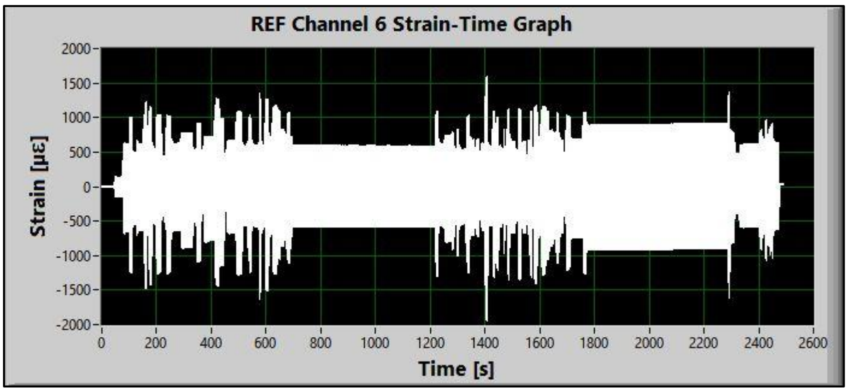

Figure A.5.3 REF Channel 6 Strain-Time Graph

APPENDIX 6: CHANNEL-2 RAINFLOW SOLUTION MATRIX

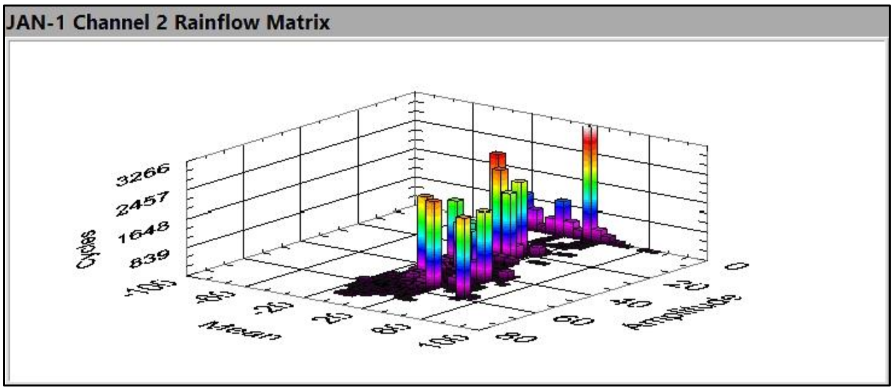

Figure A.1.1 JAN-1 Channel 2 Rainflow solution matrix

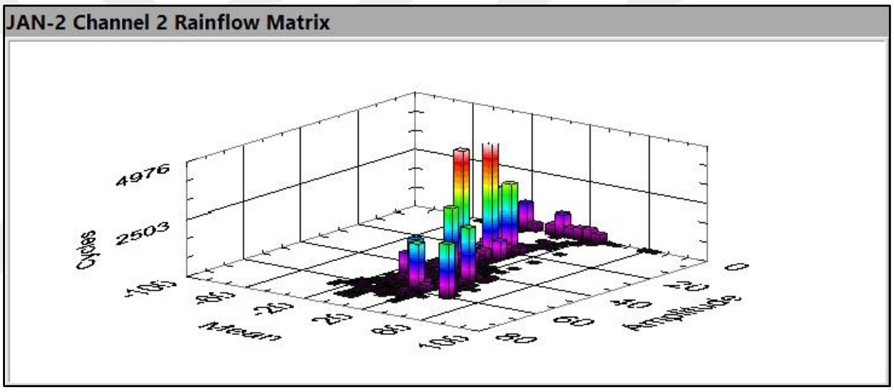

Figure A.1.2 JAN-2 Channel 2 Rainflow solution matrix

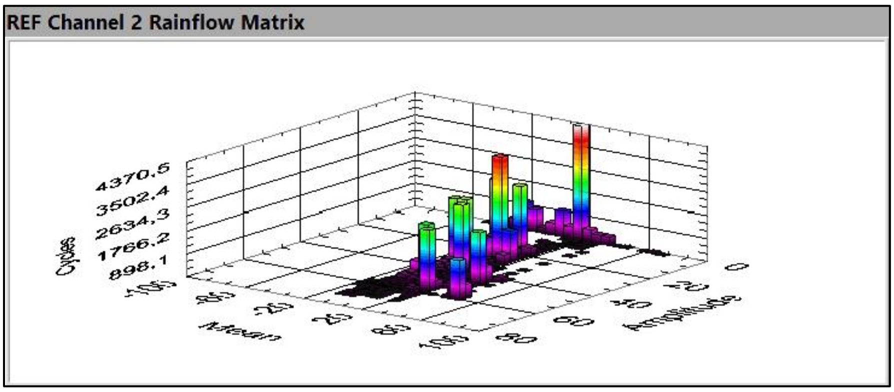

Figure A.1.2 REF Channel 2 Rainflow solution matrix

APPENDIX 7: CHANNEL-3 RAINFLOW SOLUTION MATRIX

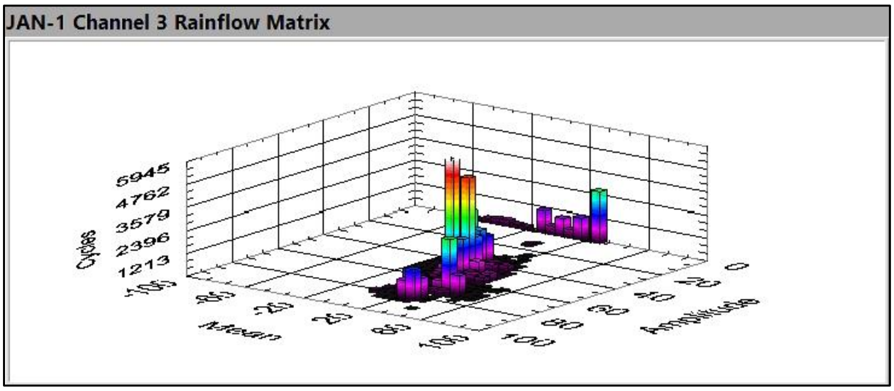

Figure A.2.1 JAN-1 Channel 3 Rainflow solution matrix

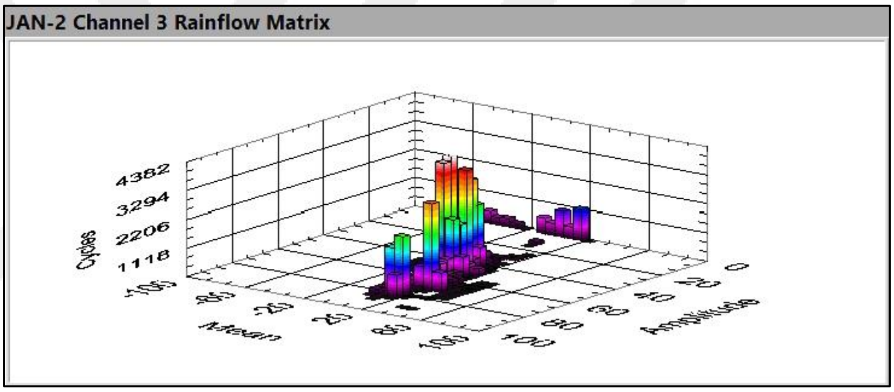

Figure A.2.2 JAN-2 Channel 3 Rainflow solution matrix

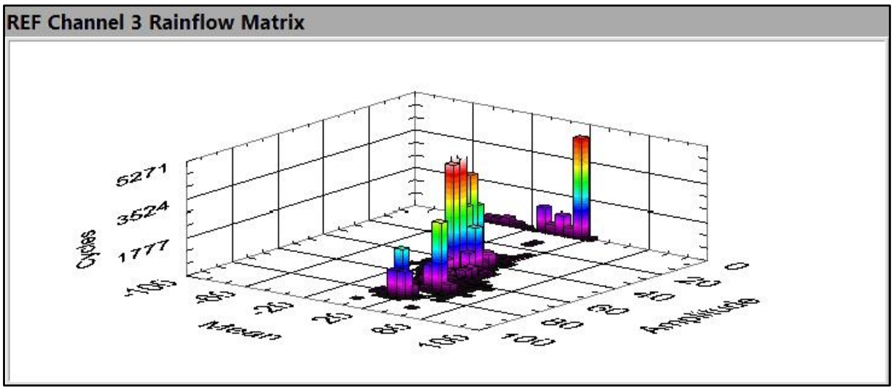

Figure A.2.3 REF Channel 3 Rainflow solution matrix

APPENDIX 8: CHANNEL-4 RAINFLOW SOLUTION MATRIX

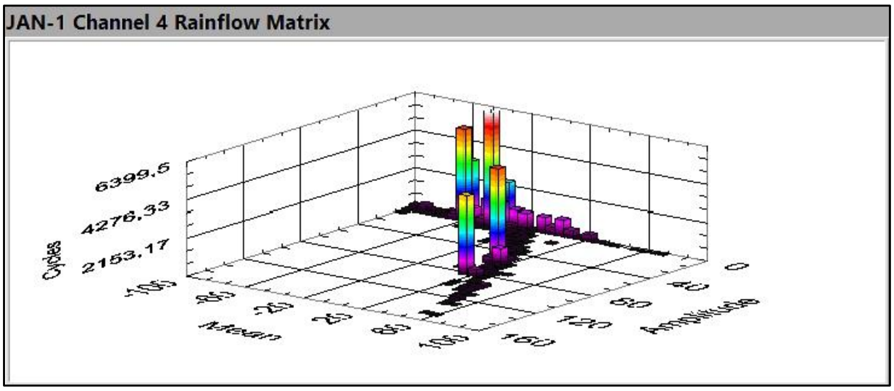

Figure A.3.1 JAN-1 Channel 4 Rainflow solution matrix

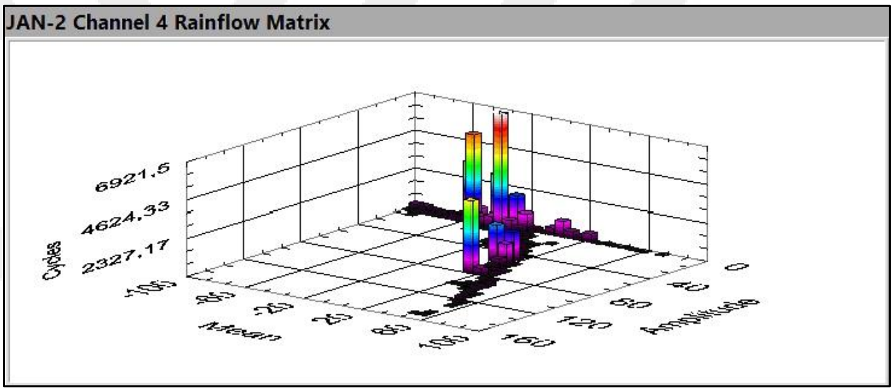

Figure A.3.2 JAN-2 Channel 4 Rainflow solution matrix

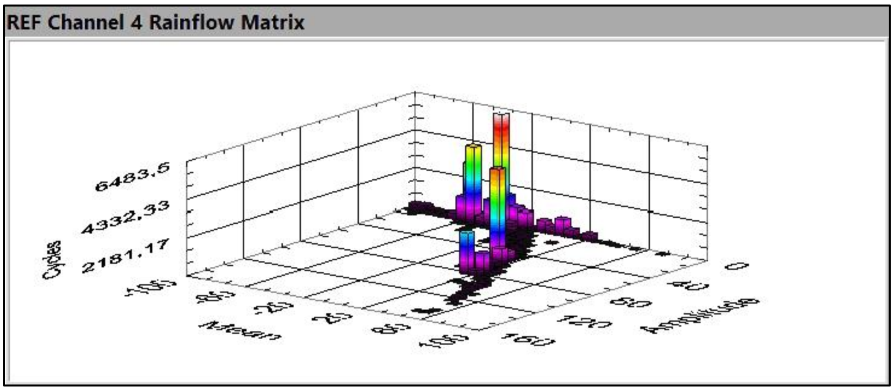

Figure A.3.3 REF Channel 4 Rainflow solution matrix

APPENDIX 9: CHANNEL-5 RAINFLOW SOLUTION MATRIX

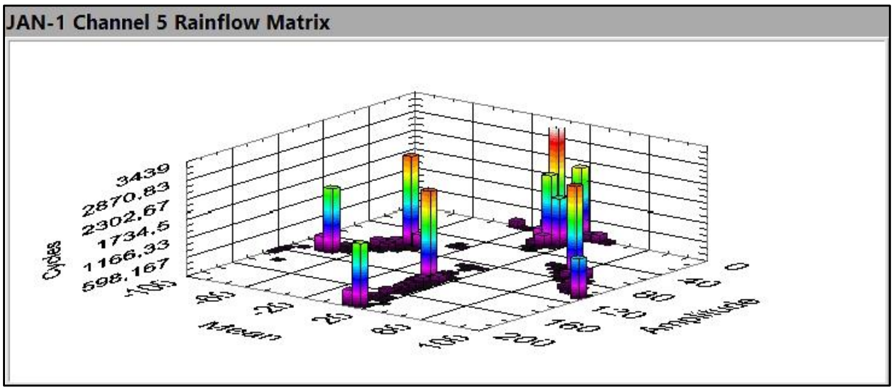

Figure A.4.1 JAN-1 Channel 5 Rainflow solution matrix

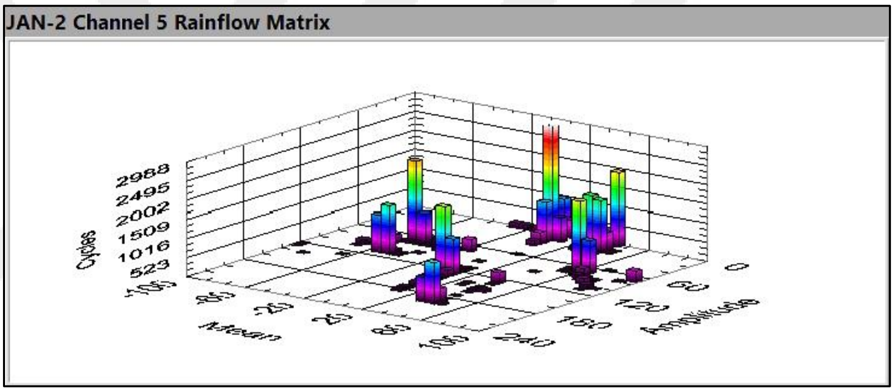

Figure A.4.2 JAN-2 Channel 5 Rainflow solution matrix

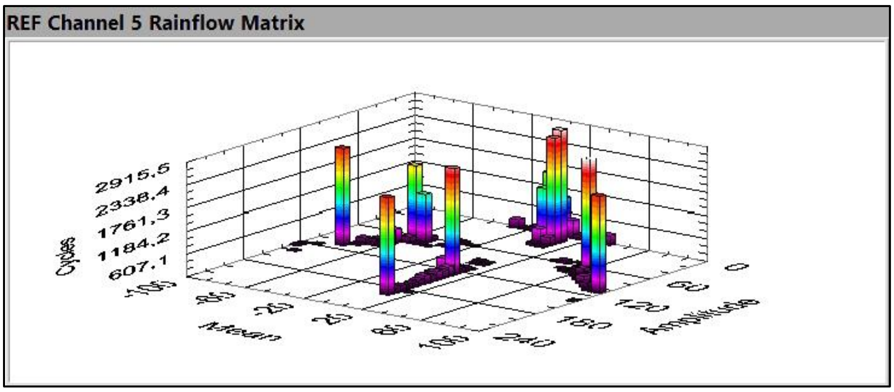

Figure A.4.3 REF Channel 5 Rainflow solution matrix

APPENDIX 10: CHANNEL-6 RAINFLOW SOLUTION MATRIX

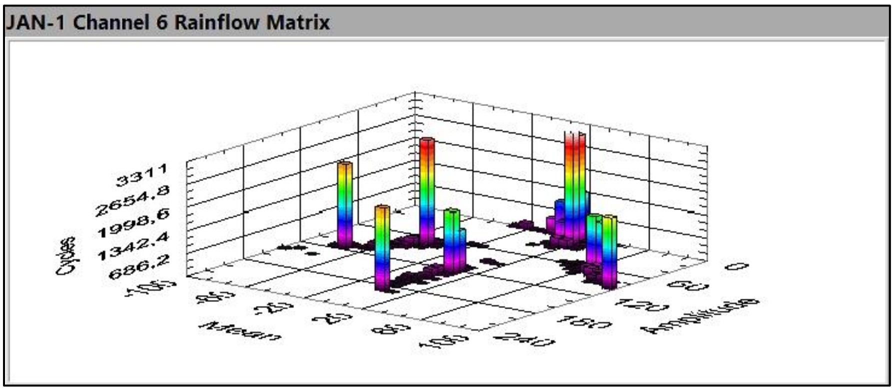

Figure A.5.1 JAN-1 Channel 6 Rainflow solution matrix

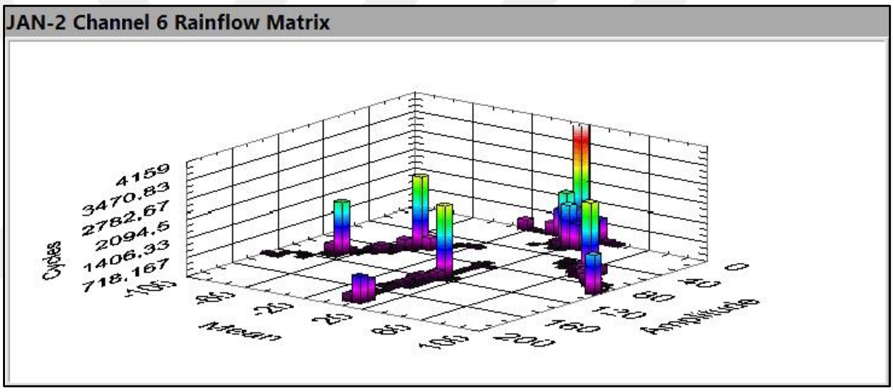

Figure A.5.2 JAN-2 Channel 6 Rainflow solution matrix

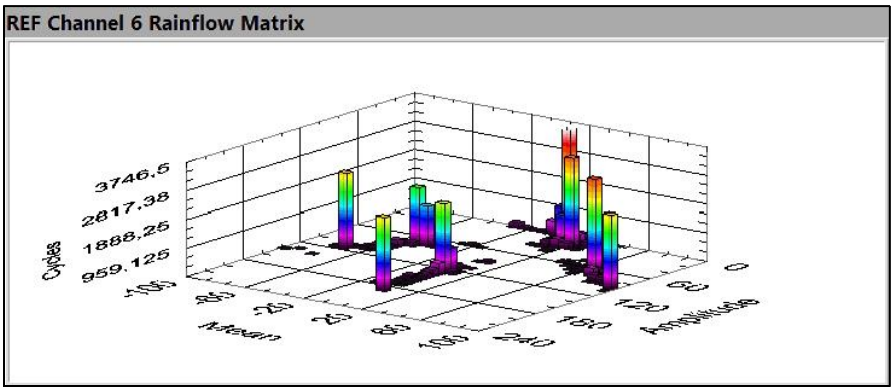

Figure A.5.3 REF Channel 6 Rainflow solution matrix